Article

Neuron

Normal CA1 Place Fields but Discoordinated Network Discharge in a *Fmr1*-Null Mouse Model of Fragile X Syndrome

Highlights

- Excessive learning-induced CA3→CA1 synaptic transmission and plasticity in FXS mice
- Place fields of individual *Fmr1*-null CA1 place cells are normal in fixed conditions
- Unstable spike-field phase organization of *Fmr1*-null CA1 place cell discharge
- Ensemble place cell discharge is weakly coordinated in *Fmr1*-null mice

Authors

Zoe Nicole Talbot, Fraser Todd Sparks, Dino Dvorak, Bridget Mary Curran, Juan Marcos Alarcon, André Antonio Fenton

Correspondence

afenton@nyu.edu

In Brief

Talbot et al. report normal location-specific hippocampus CA1 place cell responses, but dysregulated synaptic function and discoordinated spike timing in fragile X syndrome (FXS) model mice, pointing to abnormally timed interactions between normally tuned single-neuron responses in FXS-associated intellectual disability and autism.

Talbot et al., 2018, Neuron *97*, 684–697
February 7, 2018
https://doi.org/10.1016/j.neuron.2017.12.043

CellPress

CellPress

Neuron
Article

Normal CA1 Place Fields but Discoordinated Network Discharge in a *Fmr1*-Null Mouse Model of Fragile X Syndrome

Zoe Nicole Talbot,[1,7] Fraser Todd Sparks,[2,6,7] Dino Dvorak,[2] Bridget Mary Curran,[3] Juan Marcos Alarcon,[3] and André Antonio Fenton[2,4,5,8,*]

[1]School of Medicine, New York University, New York, NY 10016, USA
[2]Center for Neural Science, New York University, New York, NY 10003, USA
[3]Department of Pathology, Robert F. Furchgott Center for Neuroscience, State University of New York, Downstate Medical Center, Brooklyn, NY 11203, USA
[4]Neuroscience Institute at the New York University Langone Medical Center, New York, NY 10016, USA
[5]Department of Physiology & Pharmacology, Robert F. Furchgott Center for Neuroscience, State University of New York, Downstate Medical Center, Brooklyn, NY 11203, USA
[6]Present address: Department of Neuroscience, Columbia University Medical Center, New York, NY 10032, USA
[7]These authors contributed equally
[8]Lead Contact
*Correspondence: afenton@nyu.edu
https://doi.org/10.1016/j.neuron.2017.12.043

SUMMARY

Silence of *FMR1* causes loss of fragile X mental retardation protein (FMRP) and dysregulated translation at synapses, resulting in the intellectual disability and autistic symptoms of fragile X syndrome (FXS). Synaptic dysfunction hypotheses for how intellectual disabilities like cognitive inflexibility arise in FXS predict impaired neural coding in the absence of FMRP. We tested the prediction by comparing hippocampus place cells in wild-type and FXS-model mice. Experience-driven CA1 synaptic function and synaptic plasticity changes are excessive in *Fmr1*-null mice, but CA1 place fields are normal. However, *Fmr1*-null discharge relationships to local field potential oscillations are abnormally weak, stereotyped, and homogeneous; also, discharge coordination within *Fmr1*-null place cell networks is weaker and less reliable than wild-type. Rather than disruption of single-cell neural codes, these findings point to invariant tuning of single-cell responses and inadequate discharge coordination within neural ensembles as a pathophysiological basis of cognitive inflexibility in FXS.

INTRODUCTION

Fragile X syndrome (FXS) is a neurodevelopmental disorder and is the most common inherited form of intellectual disability and single-gene cause of autism spectrum disorder (ASD) characterized by inflexible behaviors. FXS results from silencing the X-linked *FMR1* gene and subsequent loss of its protein product fragile X mental retardation protein (FMRP) (Colak et al., 2014; Pieretti et al., 1991). FMRP is a negative regulator of protein synthesis, and because it binds to more than 400 mRNAs, the consequences of FMRP loss are diverse and not fully characterized (Brown et al., 2001; Darnell et al., 2011).

Synaptic dysfunction is the dominant hypothesis to explain the intellectual disability associated with FMRP absence, but these studies of synaptic function have only been performed in brain slices from task-naive animals (Bear et al., 2004; Waung and Huber, 2009). FMRP absence in *Fmr1*-null mice dysregulates translation of mRNAs that encode dendrite-localized proteins that contribute to synaptic development and function in both pre- and postsynaptic sites, resulting in abnormal dendritic morphology likely due to altered levels of scaffold proteins and glutamate receptors in postsynaptic densities (Bassell and Warren, 2008; Bhakar et al., 2012; Braun and Segal, 2000; Comery et al., 1997; Deng et al., 2011; Patel et al., 2013). One of the best-characterized forms of FMRP-related synaptic dysfunction in brain slices from task-naive *Fmr1*-null mice is excessive group 1 mGluR-stimulated long-term depression (mGluR-LTD), indicating that some abnormalities associated with FMRP loss depend on neural activity (Bear et al., 2004; Dölen et al., 2010; Huber et al., 2002). Although alterations in hippocampal long-term potentiation (LTP) have been elusive (Godfraind et al., 1996), abnormal features of LTP in hippocampus and neocortical circuits have also been reported in brain slices from task-naive mice after reducing or eliminating FMRP (Chen et al., 2014; Hu et al., 2008; Hunsaker et al., 2012; Larson et al., 2005; Lauterborn et al., 2007; Yun and Trommer, 2011). Abnormal activity-dependent synaptic physiology in task-naive *Fmr1*-null mice, as well as other mutant models of syndromic forms of ASD, have led synaptic dysfunction hypotheses to predict disrupted tuning of the discharge of individual neurons to represent

information that underlies intellectual ability (Zoghbi and Bear, 2012), which we will here call the "disruption hypothesis." However, learning and memory are relatively normal in *Fmr1*-null animals (Bakker et al., 1994; Bhattacharya et al., 2012; Brennan et al., 2006; D'Hooge et al., 1997; Kooy et al., 1996; Zhao et al., 2005), highlighting the gap in understanding how synaptic dysfunction, measured in task-naive mice, is related to intellectual disability in FXS and similar disorders. Accordingly, we take a systems approach to understand how FMRP loss causes intellectual disability by studying the "missing middle" level of biological function (Laughlin et al., 2000), assessed by the electrophysiology of synaptic populations (local field potentials [LFPs]) and the action potential discharge in ensembles of single neurons.

Like FXS patients (Hooper et al., 2008), *Fmr1*-null mice exhibit cognitive inflexibility (Chen et al., 2014; Kooy et al., 1996; Krueger et al., 2011). This inflexibility has been measured using dorsal hippocampus-sensitive and synaptic plasticity-dependent active place avoidance task variants that test the ability to discriminate between established and novel spatial memories (Cimadevilla et al., 2001; Hsieh et al., 2017; Kubík and Fenton, 2005; Pastalkova et al., 2006; Pavlowsky et al., 2017; Tsokas et al., 2016). *Fmr1*-null and wild-type (WT) mice learn and remember equally well the stationary location of a mild foot shock on a slowly rotating arena in the standard active place avoidance task variant. However, the *Fmr1*-null mice are impaired when required to discriminate between long-term memory of the initially learned shock location and the current shock location after the shock zone is either changed or eliminated (Radwan et al., 2016). At the same time, the spectral content of concurrently recorded LFPs along the dorsal hippocampal somatodendritic axis is indistinguishable between *Fmr1*-null and WT mice, but the somatodendritic organization of phase-amplitude coupled (PAC) 30–100 Hz gamma oscillation amplitudes and ~8 Hz theta oscillation phases is abnormal. The aberrations are extreme when cognitive inflexibility manifests in memory conflict and memory extinction tests of flexibility; whereas WT PAC is attenuated when the shock zone is changed or eliminated, *Fmr1*-null PAC persists (Radwan et al., 2016). These observations suggest an alternative "hyperstable/discoordination" hypothesis that neural information processing is excessively stable and consequently poorly coordinated in the absence of FMRP, leading to inflexible and poorly coordinated neural representations and behavior. We evaluated the disruption and the hyperstable/discoordination hypotheses, which make different predictions for how loss of FMRP affects neural information processing.

To evaluate predictions of the neural information disruption and hyperstability/discoordination hypotheses, we used the neural representation of location in the discharge of hippocampus place cells as a model of flexible cognitive information processing (Fenton, 2015a; Kelemen and Fenton, 2016; Moser et al., 2015; O'Keefe and Nadel, 1978). Whereas the disruption hypothesis asserts altered *Fmr1*-null hippocampus place coding, such as poor quality place fields, the hyperstable/discoordination hypothesis predicts normal place coding that is abnormally indifferent to environmental conditions.

RESULTS

Exaggerated Baseline and Learning-Induced Changes of Synaptic Function in *Fmr1*-Null Mice

We began by examining synaptic function in the gene knockout *Fmr1*-null mouse using *ex vivo* hippocampal slice physiology. In agreement with prior work (Franklin et al., 2014; Godfraind et al., 1996; Hu et al., 2008; Lauterborn et al., 2007), we find that CA3 Schaffer collateral to CA1 synaptic efficacy and potentiation does not differ between WT and *Fmr1*-null brain slices taken from task-naive mice (Figure 1). We then tested whether synaptic function of task-experienced mice differs, measured 1 day after memory and control training. *Fmr1*-null mice performed as well as WT mice (Figure S1) in the hippocampus- and LTP-dependent active place avoidance task (Cimadevilla et al., 2001; Pastalkova et al., 2006), replicating a prior report (Radwan et al., 2016). We observed training-induced changes in synaptic function, consistent with prior findings using extended training protocols (Park et al., 2015; Pavlowsky et al., 2017). Specifically, greater synaptic efficacy was observed in the trained WT group compared to the home cage group as well as the exposed WT control group that experienced the training environment but were never shocked (Figure 1A). Synaptic responses from the exposed *Fmr1*-null group were almost twice as large as the task-naive *Fmr1*-null and the WT groups (Figure 1B); synaptic responses in the *Fmr1*-null trained group were also enhanced, similar to the exposed *Fmr1*-null group (Figure 1B). Synaptic potentiation after 100 Hz high-frequency stimulation was indistinguishable between the WT and *Fmr1*-null task-naive home cage groups, as previously reported (Godfraind et al., 1996; Hu et al., 2008). Potentiation was also similar in the WT task-naive and exposed control groups and potentiation in these groups was greater than the potentiation in the WT trained group (Figure 1C), as has been reported after extended training (Pavlowsky et al., 2017). The early and late phases of the potentiation were increased in the exposed *Fmr1*-null group compared to the *Fmr1*-null task-naive and trained groups as well as the WT groups (Figures 1C and 1D). Moreover, the difference in the amplitude of synaptic potentiation between the WT trained and the exposed groups (Figure 1C) was substantially smaller than the difference between the *Fmr1*-null trained and the exposed and task-naive *Fmr1*-null mice (Figure 1D). These observations indicate that experience-dependent CA1 synaptic function changes are enhanced in *Fmr1*-null animals and that experience-driven modulation of CA1 synaptic function is intensified in *Fmr1*-null mice compared to mice that express FMRP.

Non-spatial and Spatial Single-Cell Discharge Features of CA1 Place Cells Are Intact in *Fmr1*-Null Mice

We then compared the characteristics of dorsal CA1 single-unit discharge in freely behaving WT and *Fmr1*-null mice in fixed environments (Figure S2). Of the 1,115 single-unit waveform clusters that were identified, 499 were recorded from 12 WT mice and 616 were recorded from 9 *Fmr1*-null mice (Table S2). When the single-unit isolation quality was sufficiently high ($Isol_{BG}$ and $Isol_{NN}$ each >4 bits) in standard recordings, these were

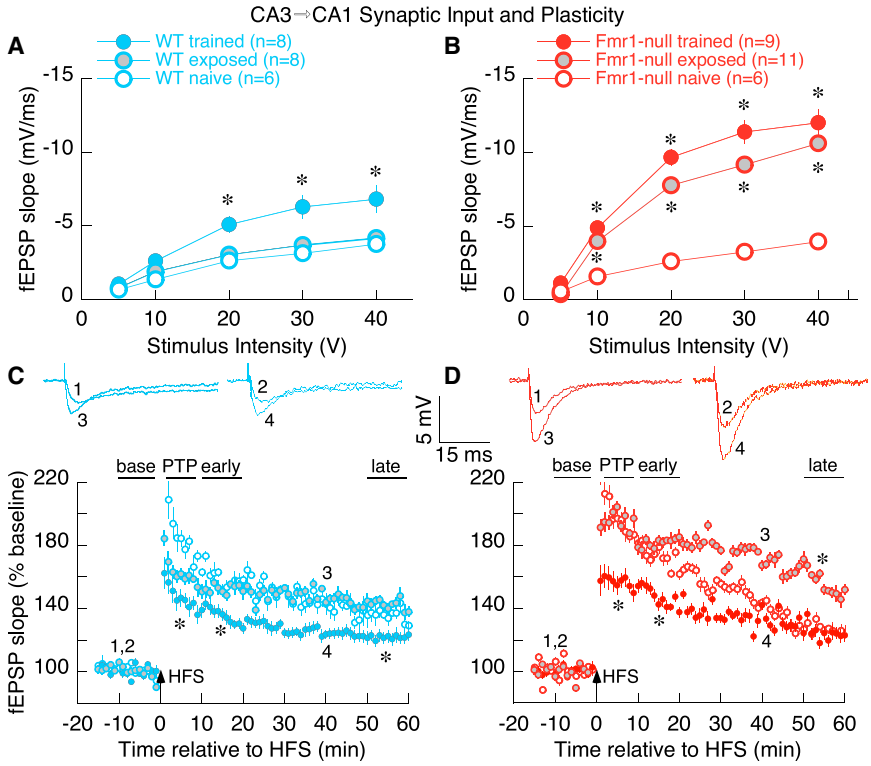

Figure 1. Abnormal Experience-Dependent Changes of Baseline and Plastic Hippocampal CA3→CA1 Synaptic Function in *Fmr1*-Null Mice

(A and B) Comparing efficacy of baseline synaptic transmission in WT (A) and *Fmr1*-null (B) mice that are either naive or after control exposure or memory training in the active place avoidance task. WT and *Fmr1*-null synaptic responses are indistinguishable in naive mice (A and B, open circles). Memory training enhances responses in both genotypes (A and B, filled colored circles); the enhancement is greater in *Fmr1*-null mice, which unlike WT, show enhancement even after control exposure (B, gray circles). Two-way genotype × training ANOVA on the area under the curve confirmed significant effects of training ($F_{2,42}$ = 25.7, p = 10^{-8}, η_p^2 = 0.55) and the genotype × training interaction ($F_{1,42}$ = 3.49, p = 0.04, η_p^2 = 0.13). Post hoc Tukey tests confirmed the pattern *Fmr1*-null naive = WT naive = WT exposed < *Fmr1*-null exposed = *Fmr1*-null trained = WT trained.

(C and D) Synaptic potentiation to 100-Hz high-frequency stimulation (HFS) in WT (C) and *Fmr1*-null (D) mice. HFS induces post-tetanic potentiation (PTP), early potentiation, and late potentiation. Potentiation at each phase appears similar in the naive WT and *Fmr1*-null mice (C and D, open circles) and similar in WT naive and exposed mice (C, open and gray circles, respectively). Potentiation is greater in exposed than naive *Fmr1*-null mice (D, open and gray circles, respectively), but not different between exposed and naive WT mice (C, open and gray circles, respectively). Potentiation is reduced in trained mice of both genotypes (C and D, filled colored circles), except late potentiation in trained and task-naive *Fmr1*-null mice is not different, but is less that in *Fmr1*-null exposed mice. The genotype × training × phase three-way repeated-measures ANOVA on synaptic plasticity showed significant effects of phase ($F_{3,40}$ = 214.2, p = 10^{-24}, η_p^2 = 1.0) and the genotype × phase ($F_{3,40}$ = 5.28, p = 0.003, η_p^2 = 0.84) and training × phase ($F_{6,80}$ = 10.6, p = 10^{-8}, η_p^2 = 0.80) interactions so each post-stimulus phase was analyzed separately by two-way genotype × training ANOVA. The *de novo* protein-synthesis-independent PTP and early-potentiation changes were greater in exposed *Fmr1*-null mice than in exposed WT mice (genotype effects—PTP: t_{42} = 2.79, p = 0.008, d = 1.4; early potentiation: t_{42} = 3.62, p = 0.0008, d = 1.9) and smaller in trained compared to naive and exposed mice for each genotype (training effects—PTP: $F_{2,42}$ = 13.72, p = 10^{-5}, η_p^2 = 0.40; early potentiation: $F_{2,42}$ = 14.42, p = 10^{-5}, η_p^2 = 0.41). *De novo* protein-synthesis-dependent late potentiation was not different between the genotypes (t_{42} = 0.84, p = 0.4, d = 0.51), but it was weakest in the trained groups (training effect: $F_{2,42}$ = 19.36, p = 10^{-6}, η_p^2 = 0.48).

*p < 0.05 relative to task naive. In (C) and (D), traces 1 and 2 represent baseline fEPSP responses and traces 3 and 4 represent potentiated fEPSP responses from exposed and trained mice, respectively.

Error bars represent SEM.

See also Figure S1.

classified as putative principal cells or interneurons. Thus, 226 WT and 334 *Fmr1*-null presumptive cells comprised the dataset and were subclassified into functional classes as place cells, putative non-spatial pyramidal cells, and putative interneurons, henceforth referred to without the "putative" adjective. A lower proportion of these were classified as interneurons in WT mice (28, 12.4%) than *Fmr1*-null mice (98, 29.3%; test of proportions z = 9.4, p = 10^{-17}). However, according to standard criteria (Figure S3) (Fenton et al., 2008; Fox and Ranck, 1975, 1981), when the putative principal cells were classified as place cells (WT n = 108 [47.8%], *Fmr1* null n = 141 [42.2%]), the prevalence was lower in the *Fmr1*-null mice (test of proportions z = 2.04, p = 0.02). The fundamental extracellular waveform and non-spatial discharge characteristics of the classified cells were indistinguishable between the genotypes (Figure S3 for firing rate, burst propensity, inter-spike interval, and firing rate comparisons). Furthermore, the fundamental measures of spatial discharge quality did not differ between either the WT and the *Fmr1*-null place cells or interneurons (Table S1). The response to changing the environment enclosure from a square to a circular cylinder also did not appear to differ between the genotypes for the subset of cells that were tested (Figure S4). Consistent with remapping, the firing rate maps recorded in the two enclosures were typically uncorrelated such that both the WT (n = 25, r = 0.054 ± 0.028, t_{24} = 1.92, p = 0.07, r^2 = 0.003) and the *Fmr1*-null (n = 31, r = 0.050 ± 0.027, t_{30} = 1.89, p = 0.07, r^2 = 0.003) distributions of rate map similarities were indistinguishable from independence, although 8/25 WT and 8/31 *Fmr1*-null place cells were significantly positively correlated (proportions test z = 0.85, p = 0.3). Importantly, the WT and *Fmr1*-null distributions of z-transformed similarity values were not distinguishable (t_{54} = 0.10, p = 0.9, d = 0.03). These findings of normal place-cell spatial firing properties are unexpected according to disruption hypotheses (Figure 2).

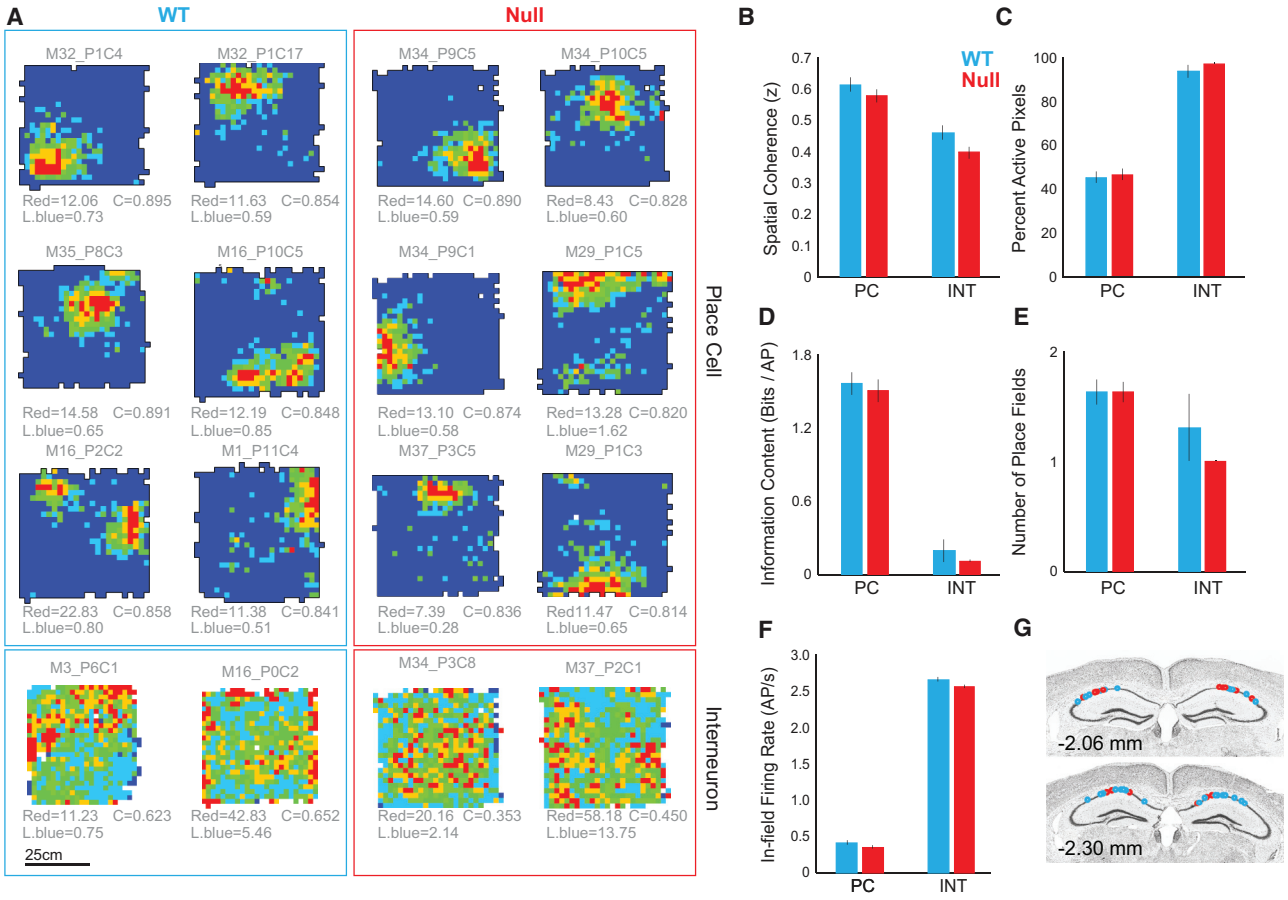

Figure 2. Similar Spatial Properties of WT and *Fmr1*-Null CA1 Place Cells and Interneurons in a Fixed Environment

Place cells and interneurons recorded in the box from the:

(A) WT and *Fmr1*-null mice. Spatial firing quality differs between place cells and interneurons, but not between genotypes, as assessed by two-way genotype × cell class ANOVAs.

(B) Spatial coherence (genotype: $F_{1,340} = 0.60$; $p = 0.44$; $\eta_p^2 = 0.0018$; cell class: $F_{2,340} = 211.2$; $p = 10^{-60}$; $\eta_p^2 = 0.55$; interaction; $F_{2,340} = 2.2$; $p = 0.11$; $\eta_p^2 = 0.013$).

(C) Proportion of the environment in which the cell discharged (genotype: $F_{1,340} = 3.7$; $p = 0.06$; $\eta_p^2 = 0.011$; cell class: $F_{2,340} = 105.2$; $p = 10^{-36}$; $\eta_p^2 = 0.38$; interaction; $F_{1,340} = 2.3$; $p = 0.10$; $\eta_p^2 = 0.013$).

(D) Information content (genotype: $F_{1,340} = 3.6$; $p = 0.06$; $\eta_p^2 = 0.011$; cell class: $F_{2,340} = 58.2$; $p = 10^{-22}$; $\eta_p^2 = 0.26$; interaction; $F_{2,340} = 2.8$; $p = 0.06$; $\eta_p^2 = 0.016$).

(E) Number of place fields (genotype: $F_{1,340} = 0.13$; $p = 0.72$; $\eta_p^2 = 0.00038$; cell class: $F_{2,340} = 4.0$; $p = 0.02$; $\eta_p^2 = 0.023$; interaction; $F_{2,340} = 2.2$; $p = 0.11$; $\eta_p^2 = 0.013$).

(F) In-field firing rate (genotype: $F_{1,340} = 0.24$; $p = 0.62$; $\eta_p^2 = 0.0011$; cell class: $F_{2,340} = 188.6$; $p = 10^{-56}$; $\eta_p^2 = 0.45$; interaction: $F_{2,340} = 0.009$; $p = 0.92$; $\eta_p^2 = 0.00004$).

(G) WT photomicrograph illustrating the placement of recording electrodes in dorsal CA1. Numbers indicate anterior-posterior Bregma coordinates.

Error bars represent SEM.

See also Figures S2 and S3.

Abnormal Spike-Field Coordination in CA1 of *Fmr1*-Null Mice

Although the power spectra of LFP oscillations recorded from the CA1 pyramidal cell layer is indistinguishable between the genotypes in ~8 Hz theta and 30–100 Hz gamma ranges (Figure S5A), the cross-frequency organization of theta and gamma oscillations differs (Radwan et al., 2016), motivating us to examine how oscillations organize the discharge of individual cells (Figure S5). Oscillations in the LFP organize discharge in cell-specific and frequency-specific patterns (Figure 3A). Because locomotion speed influences frequency and amplitude of both theta (McFarland et al., 1975) and gamma (Chen et al., 2011) oscillations, we decided to limit all spike-field analyses only to running states where speed > 2 cm/s, although all analyses led to the same conclusions when speed was limited to a narrow speed range of 2–4 cm/s (data not shown). While hyperactivity was previously associated with *Fmr1*-null behavior in open field environments (Sørensen et al., 2015), during the electrophysiological recordings, we did not observe any WT versus *Fmr1* null differences in locomotion speed or differences in the linearity (opposite of crookedness) of how the mice walked. The modulation of place cell discharge in the theta (~8 Hz) and

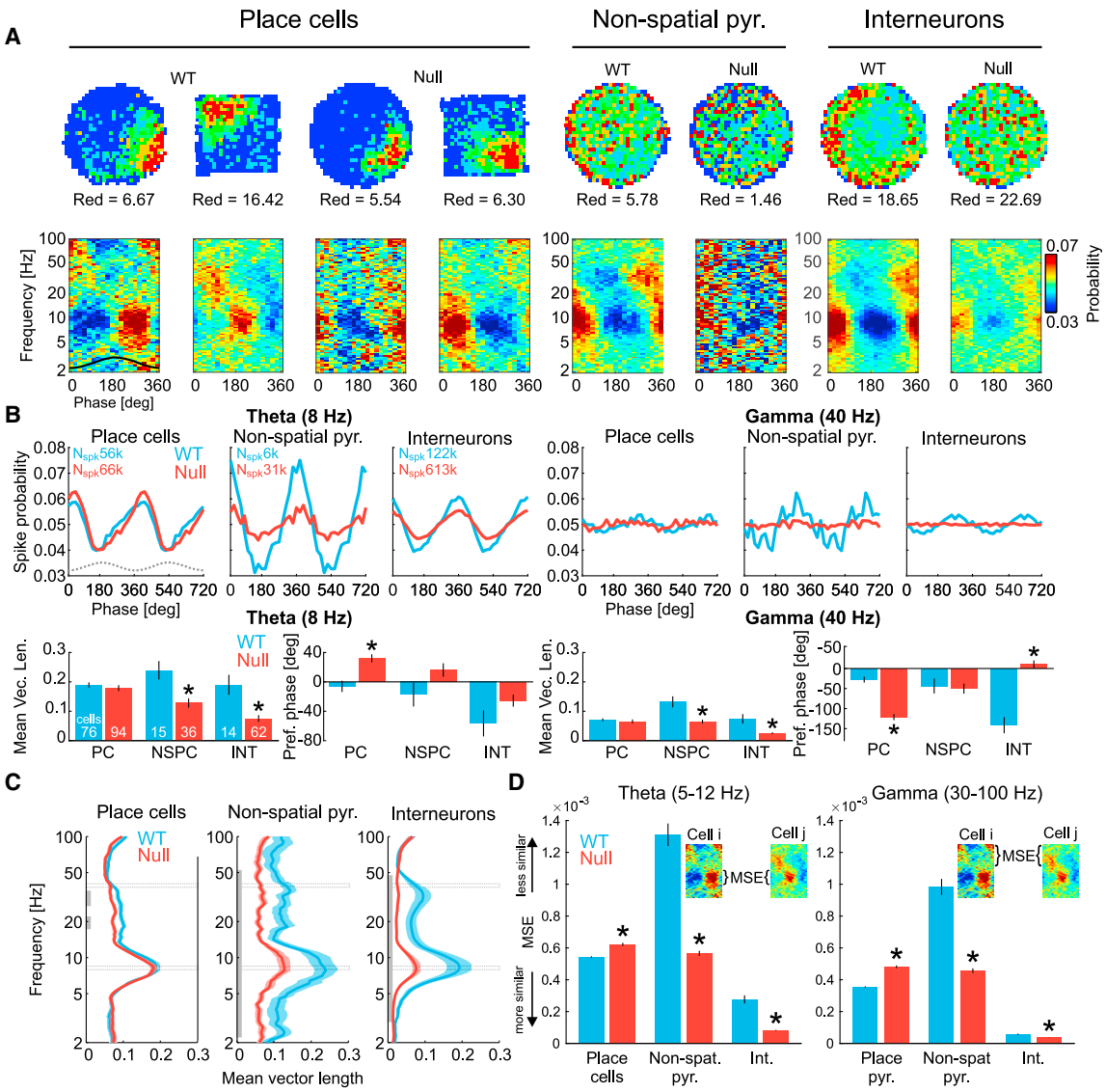

Figure 3. Abnormal Organization of *Fmr1*-Null Principal Cell Spiking by LFP Oscillations

(A) Cell-specific spatial firing rate maps and phase-frequency discharge probability histograms of place cells, non-spatial putative pyramidal cells, and putative interneurons.

(B) Top: average phase modulation of discharge probabilities for theta (8 Hz) and gamma (40 Hz) bands, computed from all spikes of the corresponding functional category. Bottom: quantification of the phase modulation estimated as mean vector length (left) and the phase preference measured as distance from trough (0°), averaged across individual cells. Cell counts are the same for the theta and gamma bands.

(C) Coupling strength between spikes and field measured as mean resultant vector length across wide-band frequencies and averaged across cells. The resultant or Rayleigh vector is a test statistic for assessing circular homogeneity. The gray vertical line indicates continuous bands with $p < 0.05$ for at least three neighboring frequencies. Gray open rectangles mark the theta and gamma frequencies that are used for the group statistics in (B).

(D) Mean square error (MSE) differences between phase-frequency discharge probability histograms across all pairs of cells for the theta (5–12 Hz; left) and gamma (30–100 Hz; right) frequency bands. Lower MSE indicates increased similarity. *$p < 0.05$ between genotypes. Note that while resultant vector length measures polar homogeneity of a sample distribution, MSE measures distinctiveness between a pair of distributions.

Error bars represent SEM.

See also Figure S5.

low gamma (~40 Hz) bands is similar between the genotypes (Figure 3B; theta: $t_{169} = 0.78$, $p = 0.44$, $d = 0.12$; gamma: $t_{169} = 0.61$, $p = 0.53$, $d = 0.09$). However, the modulation is weaker in *Fmr1*-null compared to WT non-spatial pyramidal cells (Figures 3B and 3C; theta: $t_{50} = 3.52$, $p = 0.0009$, $d = 1.03$; gamma: $t_{50} = 4.25$, $p < 0.0001$, $d = 1.15$) and interneurons (Figures 3B and 3C; theta: $t_{75} = 3.93$, $p = 0.0002$, $d = 1.04$; gamma: $t_{75} = 5.02$, $p < 0.0001$, $d = 1.08$). We next compared the discharge phase angle in the theta and gamma bands among cells of each of the three functional classes. WT place cells discharged

at the theta trough on an earlier theta phase compared to *Fmr1*-null place cells (Figure 3B; WT: 353.9° ± 67.3°, *Fmr1* null: 32.1° ± 53.1°; Watson-Williams multi-sample test for equal means $F_{1,169} = 8.97$, $p = 0.003$, $d = 5.39$). In the gamma range, WT place cells discharged on a later gamma phase compared to *Fmr1* null (Figure 3B; WT: 332.2° ± 63.6°, *Fmr1* null: 238.8° ± 74.5°, $F_{1,169} = 26.88$, $p = 10^{-7}$, $d = 1.34$) while WT interneuron cells discharged on an earlier gamma phase compared to *Fmr1* null (WT: 218.6° ± 75.0°, *Fmr1* null: 10.6° ± 76.4°, $F_{1,75} = 10.52$, $p = 0.002$, $d = 2.75$). The strength of phase modulation of spiking across the full LFP oscillation frequency spectrum is shown in Figure 3C for the three functional classes, illustrating that there are clear genotypic differences, with a general tendency for *Fmr1*-null cells to be more weakly modulated than the WT counterpart.

We then investigated the heterogeneity of the phase-frequency discharge probability relationships among cells of each of the three functional classes in the theta and gamma bands by computing the mean-square error (MSE) between the phase-frequency discharge probability histograms of all pairs of cells (Figure 3D). These relationships were the most stereotyped (corresponding to low MSE) for interneurons in both genotypes while the relationships were the least stereotyped (corresponding to high MSE) for non-spatial pyramidal cells in both genotypes. The relationship was more stereotyped in WT compared to *Fmr1*-null place cells in the theta (5–12 Hz) and gamma (30–100 Hz) frequency ranges (Figure 3D; theta: $t_{7219} = 6.16$; $p = 10^{-10}$, $d = 0.14$; gamma: $t_{7219} = 11.32$; $p = 10^{-29}$, $d = 0.27$). The non-spatial pyramidal cells and interneurons were more stereotyped in *Fmr1*-null mice compared to WT mice in both the theta and gamma ranges (Figure 3D; theta: non-spatial pyramidal cells: $t_{733} = 15.30$; $p = 10^{-46}$, $d = 1.61$; interneurons: $t_{1980} = 14.46$; $p = 10^{-45}$, $d = 1.55$; gamma: non-spatial pyramidal cells: $t_{733} = 12.92$; $p = 10^{-34}$, $d = 1.36$; interneurons: $t_{1980} = 5.02$; $p = 10^{-7}$, $d = 0.54$). These data indicate that while individual place cells in the *Fmr1*-null mice are less organized by the phase of theta and gamma oscillations in the LFP than in WT mice, the *Fmr1*-null non-place encoding pyramidal cells and interneurons are nonetheless more stereotyped in the particular ways that spiking is organized by the oscillations that arise from population synaptic activity.

Reduced Spatial Discharge Coordination and Weaker Network States in the Short-Timescale Discharge Dynamics of *Fmr1*-Null Place Cells

We next examined the reliability of spatial discharge by measuring overdispersion during passes through the place fields (Fenton et al., 2010; Fenton and Muller, 1998; Jackson and Redish, 2007). The overdispersion of WT mouse place cells in standard environments was comparable to what has been reported for rats (Fenton et al., 2010; Fenton and Muller, 1998; Hok et al., 2012; Jackson and Redish, 2007). Overdispersion was lower (spatial firing was more reliable) in *Fmr1*-null mice when the unit of analysis is a pass through a place field (WT n = 6,776 passes, $\sigma^2 = 5.81$; *Fmr1* null n = 9,102 passes, $\sigma^2 = 4.89$) compared by parametric statistics (F test: $F_{6775,9101} = 1.19$, $p = 10^{-17}$) and non-parametric statistics (Levene's test $F_{1,15874} = 22.21$, $p = 10^{-6}$). Overdispersion was also marginally lower in *Fmr1*-null mice when the unit of analysis is a place cell (WT: n = 80; $\sigma^2 = 5.98 \pm 0.44$; *Fmr1* null: n = 98; $\sigma^2 = 5.02 \pm 0.3$; $t_{176} = 1.87$, one-tailed $p = 0.03$; Mann-Whitney U = 3,386, one-tailed $p = 0.06$, $d = 0.28$).

This greater spatial discharge reliability of individual *Fmr1*-null place cells is accompanied by significantly less spatial discharge covariance (Figure 4A) of the *Fmr1*-null cell pairs with overlapping place fields and at least 30 passes through both firing fields (Figure 4B; n = 249 pairs, average r = 0.04 ± 0.01) compared to WT cell pairs (n = 109 pairs, average r = 0.09 ± 0.03; $t_{356} = 2.39$ $p = 0.02$; Mann-Whitney U = 12,424, $p = 0.2$, $d = 0.27$). Moreover, this genotypic difference in cell-pair discharge covariance disappears after random permutations to disrupt the correspondence between the normalized firing values (z) for the cells in each pair, confirming that the cell-pair covariance difference is unlikely to be spurious ($t_{356} = 0.8$ $p = 0.4$; Mann-Whitney U = 5,834; $p = 0.9$). In fact, the difference is maintained when at least 40 qualified passes were required, providing increased confidence in the covariance estimates (WT n = 56 pairs, *Fmr1* null n = 173 pairs, average WT r = 0.19 ± 0.04, *Fmr1* null r = 0.06 ± 0.01; $t_{227} = 4.2$ $p = 10^{-4}$; Mann-Whitney U = 3,791; $p < 0.01$, $d = 0.62$). These findings indicate that loss of FMRP selectively reduces the positively coordinated firing rate fluctuations between place cells on the timescale of the 1–5 s that it takes to traverse a firing field (Fenton and Muller, 1998).

We continued by examining whether *Fmr1*-null place cells form weaker network states as suggested by this weak spatial discharge coordination. The location-independent, timescale-specific Kendall's correlation (τ) between each pair of simultaneously recorded principal cells directly estimates the strength of the network states (Neymotin et al., 2017; Schneidman et al., 2006). At the 25 ms (Figures 4C and 4D) and 40 ms timescales of gamma oscillations, as well as the 125 ms timescale of theta oscillations, *Fmr1*-null cell pair discharge correlations (n = 504 pairs) were significantly weaker than those of WT cell pairs (n = 247 pairs; Figure 4D; $\Delta t = 25$ ms: WT $\tau = 0.017 \pm 0.006$, *Fmr1* null $\tau = 0.009 \pm 0.0012$, Mann-Whitney U = 51,894, $p = 0.0002$, $d = 0.15$; $\Delta t = 40$ ms: WT $\tau = 0.02 \pm 0.007$, *Fmr1* null $\tau = 0.01 \pm 0.002$, Mann-Whitney U = 53,512, $p = 0.002$, $d = 0.14$; $\Delta t = 125$ ms: WT $\tau = 0.02 \pm 0.008$, *Fmr1* null $\tau = 0.017 \pm 0.003$, Mann-Whitney U = 55,708, $p = 0.02$, $d = 0.11$). The same trend was observed at 1 s and 5 s timescales; however, the differences did not reach significance ($\Delta t = 1$ s: WT $\tau = 0.04 \pm 0.01$, *Fmr1* null $\tau = 0.03 \pm 0.005$, Mann-Whitney U = 60,801, $p = 0.6$, $d = 0.09$; $\Delta t = 5$ s: WT $\tau = 0.03 \pm 0.01$, *Fmr1* null $\tau = 0.01 \pm 0.008$, Mann-Whitney U = 60,313, $p = 0.5$, $d = 0.13$). Thus, weaker network states of principal cell discharge result from loss of FMRP at sub-second timescales of gamma and theta oscillations. These states are also less likely to recur in *Fmr1*-null ensembles compared to WT ensembles, estimated by Pearson's correlation of the vector of Kendall correlations from the two halves of a recording, known as population coordination (PCo; Neymotin et al., 2017). Not only was WT PCo greater at the various timescales, but pairwise t tests could not reject the hypothesis that the WT vector of Kendall correlations from the two halves of a recording are the same whereas the corresponding *Fmr1*-null comparisons were all significantly different, indicating the *Fmr1*-null-correlated discharge activity was unstable at timescales from 25 ms to 5 s in comparison to

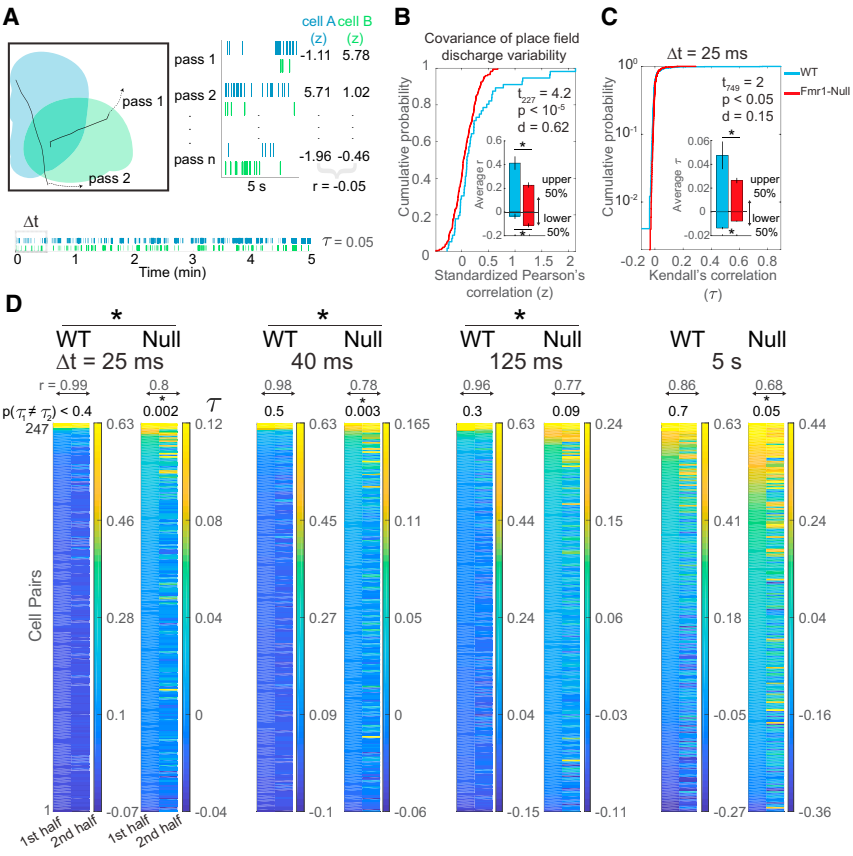

Figure 4. Weak Network States of *Fmr1* Null Place Cell Ensembles Estimated by the Set of Spike Train Correlations

(A) Schematic illustrating two place cell firing fields that are overlapping, with two 5 s trajectories that pass through both fields. Bottom: 5-min spike rasters from example cells. Right: a 5 s raster subsample with corresponding standardized firing (z) values depicted for n passes.

(B) Pearson's correlation of the two sets of z values describes the covariance of the place field discharge variability between the two cells. These WT and *Fmr1*-null cumulative probability distributions of all the pairwise correlations illustrate reduced covariance of the *Fmr1*-null place field discharge variability (t_{227} = 4.2 p = 10^{-4}; Mann-Whitney U = 3,791; p < 0.01, d = 0.62). Inset shows average Pearson's correlation for the upper and lower 50% of the distribution, which indicates that the genotypic difference is due to the more strongly coupled cell pairs (upper 50% of distribution: t_{113} = 5, p < 10^{-5}, Mann-Whitney U = 723, p = 0.001, d = 0.47; lower 50% of distribution, t_{112} = 3.1, p = 0.002, Mann-Whitney U = 747, p = 0.003, d = 0.11).

(C) Weaker temporal coupling within *Fmr1*-null place cell ensembles compared to WT ensembles measured by Kendall's correlation (τ), here assessed at the gamma Δt = 25 ms timescale. Inset shows average correlation for the upper and lower 50% of the distribution indicates that the genotypic difference is due to less extreme strongly coupled cell pairs, as well as less extreme weakly coupled cell pairs, in *Fmr1*-null mice (upper 50% of distribution, t_{374} = 2.5, p < 0.01, WT n = 124, *Fmr1* null = 252, Mann-Whitney U = 13,774, p = 0.06, d = 0.17; lower 50% of distribution, t_{373} = 6.4, p < 3 × 10^{-10}, WT n = 123, *Fmr1* null = 252, Mann-Whitney U = 8,390, p = 5.5 × 10^{-13}, d = 0.57).

(D) Kendall's correlation computed at a particular resolution (Δt) estimates coupling of the two spike trains. Each pair of columns depicts the two population correlation (PCorr) vectors of τ between the set of simultaneously recorded place-cell spike trains during 5 min intervals (PCorr vectors of *Fmr1*-null cell pairs were downsampled to 247 for better visual comparison with WT only, total n = 504; each color scale set to 70% max and min τ value of respective PCorr vectors). The correlations from the earlier interval are sorted high to low and the cell-pair identities are preserved across intervals to illustrate the recurrence of the network state that the vectors estimate. Recurrence is estimated by the PCo, Pearson correlation of the two PCorr vectors (r), which is given at the top of each vector pair. Across the gamma (25 and 40 ms), theta (125 ms) and behavioral (5 s) timescales, positive correlations between *Fmr1*-null place cells tend to be less prevalent, and the network state is less likely to recur (df = 246 and 503 for the WT and *Fmr1* null, respectively; Δt = 25 ms: t_{749} = 2.0, p = 0.05, Mann-Whitney U = 51,894, p = 0.0002, d = 0.15; Δt = 40 ms: t_{749} = 1.8 p = 0.07, Mann-Whitney U = 53,512, p = 0.002, d = 0.14; Δt = 125 ms: t_{749} = 1.4, p = 0.16, Mann-Whitney U = 55 708, p = 0.02, d = 0.11; Δt = 250 ms: t_{749} = 1.2, p = 0.2, Mann-Whitney U = 57,466, p = 0.09, d = 0.09; Δt = 1 s: t_{749} = 1 p = 0.3, Mann-Whitney U = 60,801, p = 0.6, d = 0.09; Δt = 5 s: t_{749} = 1.6, p < 0.1, Mann-Whitney U = 60,313, p = 0.5, d = 0.13). The p value for the paired t test comparison between the two halves of the recording is given at the top of each PCorr pair to estimate the recurrence of the correlations across the two halves of the recording (Δt = 25 ms: WT t_{246} = 0.9, p = 0.4; *Fmr1* null t_{503} = 3.03, p = 0.002, d = 0.12; Δt = 40 ms: WT t_{246} = 0.6, p = 0.5; *Fmr1* null t_{503} = 3, p = 0.003, d = 0.12; Δt = 125 ms: WT t_{246} = 1.02, p = 0.3; *Fmr1* null t_{503} = 1.7, p = 0.09, d = 0.07; Δt = 250 ms: WT t_{246} = 1.0, p = 0.3; *Fmr1* null t_{503} = 2.4, p = 0.02, d = 0.06; Δt = 1 s: WT t_{246} = 0.9, p = 0.4; *Fmr1* null t_{503} = 2.6, p = 0.001, d = 0.06; Δt = 5 s: t_{246} = 0.3, p = 0.7; *Fmr1* null t_{503} = 2.0, p = 0.046, d = 0.11). *p < 0.05 between genotypes.

WT (Figure 4D). These genotypic differences were unlikely to be due to differences in locomotion because the changes in locomotion across the two halves of the session were not distinct between the WT and *Fmr1*-null mice (Figure S5B; genotype: $F_{1,27}$ = 0.94, p = 0.94, η_p^2 = 0.005; epoch: $F_{1,27}$ = 7.39, p = 0.01, η_p^2 = 0.012; interaction: $F_{1,27}$ = 2.16, p = 0.15, η_p^2 = 0.012).

Similar to place cell ensembles, *Fmr1*-null cell pair discharge correlations of non-spatial pyramidal cells (n = 203 pairs) were significantly weaker than those of WT cell pairs (n = 252 pairs; Δt = 25 ms: WT τ = 0.03 ± 0.006, *Fmr1* null τ = 0.007 ± 0.002, Mann-Whitney U = 22,437, p = 0.03, d = 0.28; Δt = 40 ms: WT τ = 0.03 ± 0.006, *Fmr1* null τ = 0.008 ± 0.002, Mann-Whitney U = 22,318, p = 0.02, d = 0.26; Δt = 125 ms: WT τ = 0.04 ± 0.007, *Fmr1* null τ = 0.01 ± 0.003, Mann-Whitney U = 21,745, p = 0.007, d = 0.29). The same trend was observed at 1 s and 5 s timescales; however, 5 s differences did not reach significance (Δt = 1 s: WT τ = 0.06 ± 0.008, *Fmr1* null τ = 0.03 ± 0.007, Mann-Whitney U = 21,977, p = 0.01, d = 0.24; Δt = 5 s: WT τ = 0.08 ± 0.009, *Fmr1* null τ = 0.05 ± 0.01, Mann-Whitney U = 23,333, p = 0.12, d = 0.12). Thus, weaker network states of non-spatial principal cell discharge result from loss of FMRP at sub-second timescales of gamma and theta oscillations, as well as behavioral timescales.

To test whether these findings of weaker network states are general or specific for the active behaviors in the arena, we also examined the spike train correlations in the subset of place

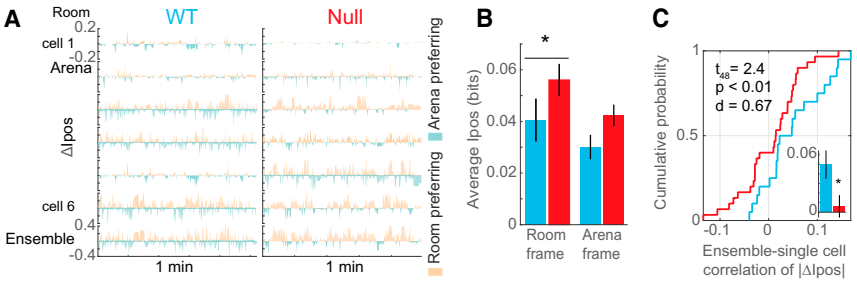

Figure 5. Abnormal Spatial Frame-Specific Place Cell Discharge in *Fmr1*-Null Place Cells during Environmental Dissociation

(A) WT and *Fmr1*-null single-cell examples of ΔI_{pos} time series illustrating the spatial frame-specific positional information alternation between the stationary room and rotating arena frames. I_{pos} is computed at 133 ms resolution. Each time series depicts the cell-specific difference between I_{pos} in the room frame and I_{pos} in the arena frame (ΔI_{pos}). The ensemble ΔI_{pos} time series is depicted on the bottom row.

(B) Average ± SEM of the room-specific and arena-specific I_{pos} values for WT (n = 20 cells) and *Fmr1* null (n = 31 cells). Room-specific I_{pos} is greater in *Fmr1* null compared to WT (Mann-Whitney U = 208, $p < 0.05$, d = 0.45) whereas arena-specific I_{pos} is only marginally greater in *Fmr1* null (Mann-Whitney U = 213, p = 0.06, d = 0.57).

(C) Cumulative probability distributions and average ± SEM (inset) summarizing the correlations of frame-specific positional discharge fluctuations $|\Delta I_{pos}|$ between single place cells and the rest of the ensemble (WT n = 20, *Fmr1* null n = 30, $t_{48} = 2.4$, $p < 0.01$, d = 0.67). *$p < 0.05$ between genotypes. Error bars represent SEM.

See also Figure S6.

cells (WT: n = 125 cell pairs from 35 cells in 6 mice; *Fmr1* null: n = 195 cell pairs from 39 cells in 4 mice) that were also recorded during quiet wakefulness and sleep. Spike train correlations did not differ at the gamma timescale (Δt = 25 ms: WT τ = 0.007 ± 0.002, *Fmr1* null τ = 0.006 ± 0.002 Mann-Whitney U = 11,248, p = 0.24, d = 0.06; Δt = 40 ms: WT τ = 0.01 ± 0.003, *Fmr1* null τ = 0.007 ± 0.003 Mann-Whitney U = 11,026, p = 0.15, d = 0.09), whereas the *Fmr1*-null correlation distribution was weaker at theta and 1 s timescales (Δt = 125 ms: WT τ = 0.015 ± 0.006, *Fmr1* null τ = 0.006 ± 0.005, Mann-Whitney U = 10,583, $p < 0.05$, d = 0.13; Δt = 250 ms: WT τ = 0.02 ± 0.007, *Fmr1* null τ = 0.006 ± 0.006, Mann-Whitney U = 10,397 p = 0.03, d = 0.14; Δt = 1 s: WT τ = 0.02 ± 0.01, *Fmr1* null τ = 0.002 ± 0.01, Mann-Whitney U = 10,629, $p < 0.05$, d = 0.13; Δt = 5 s: WT τ = 0.02 ± 0.014, *Fmr1* null $\tau = 3 \times 10^{-5}$ ± 0.012, Mann-Whitney U = 10,917, p = 0.12, d = 0.10). These genotypic differences were mainly due to lower *Fmr1*-null correlations in the lower half of the distribution (data not shown). These findings during quiet behaviors confirm that network states are weaker in the interactions among *Fmr1*-null place cells across multiple behavior states but should be interpreted with caution because genotypic differences in behaviors and sleep stages were not investigated during the analyzed period of quiet behaviors.

During Dissociation of Spatial Frames, the Fluctuations of Spatial-Frame-Specific Place Cell Discharge Is More Weakly Coordinated in *Fmr1*-Null Than in Wild-Type Ensembles

Continuous rotation of the circular arena dissociates the environment into the spatial frames of the stationary room and the rotating arena, allowing us to examine the ability of place cell ensembles to dynamically switch between representing locations in the dissociated spatial frames on sub-second timescales (Kelemen and Fenton, 2010, 2016). Although mice in the rotating arena were not performing an explicit navigation or spatial memory task and were not shocked or otherwise manipulated, place cell discharge alternated between signaling locations in the stationary and rotating spatial frames in both genotypes (Figure 5). The session-averaged, frame-specific spatial firing was better organized in the room frame, and this preference was similar for the two genotypes (Figure S6). Figure 5A illustrates the dynamics of frame-specific discharge during rotation, measured as the time series of ΔI_{pos}. This frame specificity spontaneously alternates between the stationary and rotating frames and is overall stronger in the *Fmr1*-null mice compared to WT (Figure 5B). Place cells from both genotypes tended to preferentially signal stationary locations over rotating locations.

We then examined how well these dynamics were correlated among the network of cells by asking how the frame-specific spatial coding dynamics of a single cell is correlated with the frame-specific spatial coding fluctuations of the remaining ensemble of cells. The ensemble fluctuations of frame-specific discharge ($|\Delta I_{pos}|$) were computed for all simultaneously recorded cells except one, and the correlation of the ensemble and "left-out" single-cell $|\Delta I_{pos}|$ time series was calculated. The association between the ensemble and the single left-out cell was weaker in *Fmr1*-null compared to WT place cells (Figure 5C), further indicating weaker network states in the *Fmr1*-null mice.

Correlated Network Discharge Predicts Cognitive Performance

Finally, we explored whether the estimates of neural coordination that can distinguish *Fmr1*-null and WT mice can also predict cognitive ability. Nine of the mice (5 WT and 4 *Fmr1* null) from which we recorded place cell ensemble activity also subsequently received active place avoidance training to assess their cognitive ability (Figure 6). We took the most commonly used measure of place avoidance, the number of errors (entrances to the shock zone) during training, as an index of cognitive ability that did not differ between the genotypes. Despite the modest number of subjects, this index of poor performance was positively correlated with inconsistently coordinated discharge during passes across the firing fields of pairs of place cells, which was estimated by the correlating avoidance performance with the SEM of the covariance in place cell discharge as the mouse traverses a pair of firing fields (e.g., Figure 4B; r = 0.61, p = 0.04, r^2 = 0.37). This relationship hints that poor cognitive performance may be associated with weakly correlated network discharge. We thus examined the extent to which place avoidance

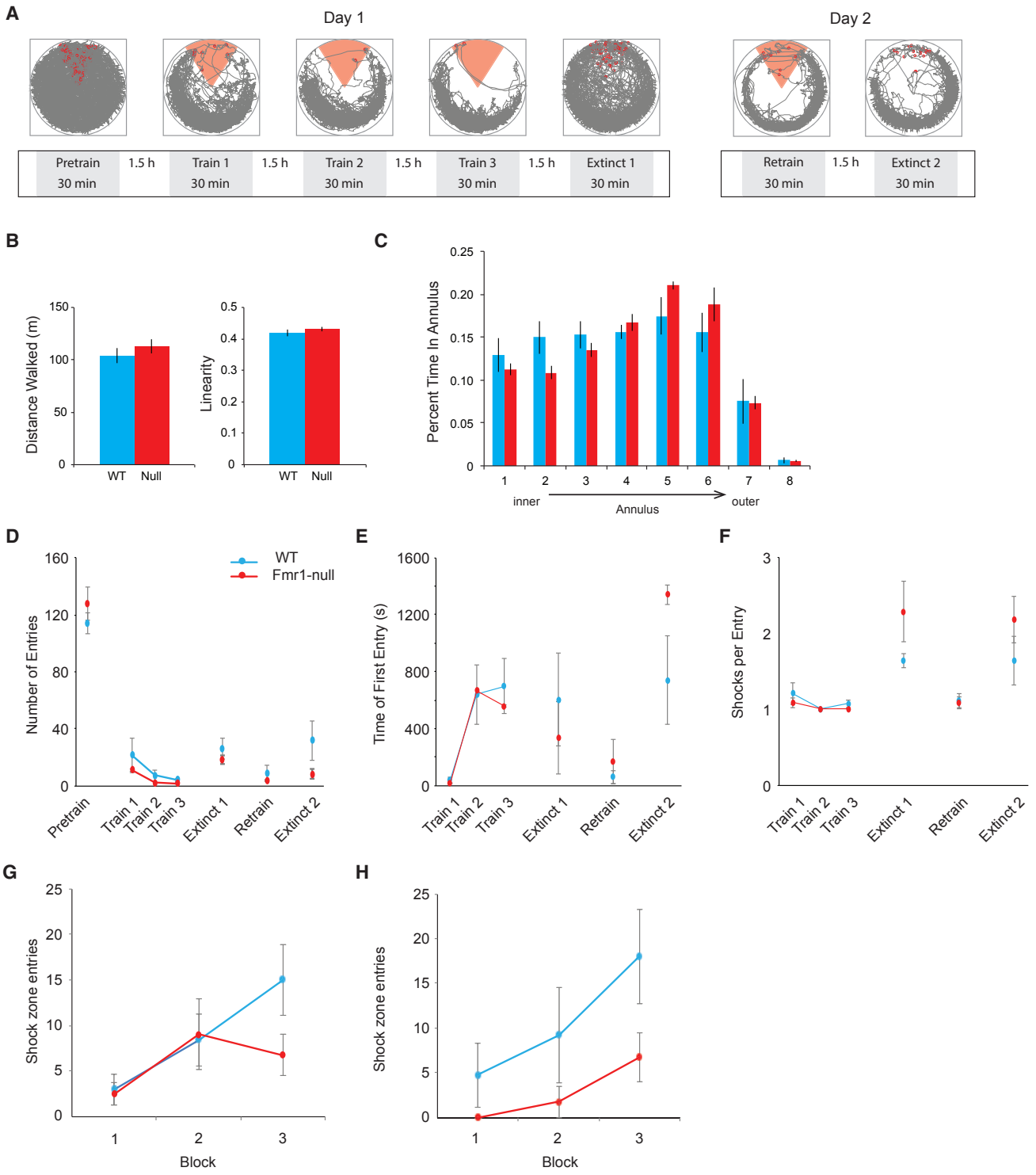

Figure 6. Active Place Avoidance Behavior of a Subset of Mice that Contributed Single-Unit Data

(A) Schematic of active place avoidance experimental design with examples of the mouse's path to illustrate spatial occupancy. On day 1, WT (n = 5) and *Fmr1*-null (n = 4) mice were first habituated to the rotating arena in a pretraining trial before receiving three trials of avoidance training with shock turned on, after which an extinction trial was conducted with the shock off. On day 2, mice were first retrained in one trial before a second extinction trial was conducted. The red sector indicates the active shock zone.

(B) During pretraining open field behavior, there were no genotype differences in total distance traveled ($t_7 = 1.03$, $p = 0.5$, $d = 0.88$) or linearity of motion ($t_7 = 2.97$, $p = 0.2$, $d = 0.50$).

(legend continued on next page)

performance can be predicted from the average Kendall correlation among the pairs of place cells that were recorded from a single mouse (e.g., Figures 4C and 4D), because this value estimates the strength of correlated network activity (Schneidman et al., 2006). Indeed, place avoidance performance was negatively correlated with Kendall's correlation; the relationship was strongest at the gamma and theta timescales of 25 ms ($r = -0.87$, one-tailed $p = 0.001$, $r^2 = 0.75$), 40 ms ($r = -0.80$, one-tailed $p = 0.005$, $r^2 = 0.63$), and 125 ms ($r = -0.62$, one-tailed $p = 0.04$, $r^2 = 0.38$), whereas the relationship was no longer significant at 250 ms ($r = -0.47$, 1-tailed $p = 0.1$, $r^2 = 0.22$) timescales and longer.

DISCUSSION

Experience-Dependent Synaptic Function Abnormalities and Intact Place Cell Tuning in *Fmr1*-Null Mice

The basic place cell properties that we measured are disrupted by a variety of genetic manipulations that affect synaptic plasticity, including deletion of NMDA receptors (Dragoi and Tonegawa, 2013; McHugh et al., 1996, 2007; Nakazawa et al., 2002, 2003), the kinases PKA (Rotenberg et al., 2000), and CaMKII (Cho et al., 1998; Rotenberg et al., 1996), but effects of *Fmr1* deletion on hippocampal information processing during behavior have not been previously described. The absence of the gene product FMRP dysregulates translation of hundreds of mRNAs, modifying the expression of channel proteins (Brown et al., 2001; Gross et al., 2011) and altering neuronal excitability and synaptic function in hippocampus and possibly throughout the brain as assessed by *in vitro* studies (Deng et al., 2011; Gibson et al., 2008; Zhang and Alger, 2010; Zhong et al., 2010). Such consequences have motivated disruption hypotheses that predict impaired information processing in the neural networks of individuals without FMRP. However, the present findings appear incompatible with disruption hypotheses and strongly support alternative hyperstable/discoordination hypotheses for the consequences of FMRP loss in a neural circuit leading to intellectual disability in FXS. While we confirmed that Schaffer collateral synaptic transmission and plasticity are indistinguishable between naive WT and *Fmr1*-null brain slices as previously reported (Franklin et al., 2014; Godfraind et al., 1996; Hu et al., 2008; Lauterborn et al., 2007), we also uncovered substantial abnormalities in the *Fmr1*-null mice, but only after spatial experience (Figure 1). The experience-dependent increase in synaptic transmission and synaptic plasticity was observed 24 hr after active behavior in a novel environment as we have shown before in WT mice (Pavlowsky et al., 2017), but the changes are excessive in *Fmr1*-null mice. The excessive changes manifest whether or not place learning was conditioned whereas WT mice only express such changes after conditioning (Figure 1). This, the first demonstration of these abnormalities of the *Fmr1*-null mouse, is consistent with reduced translation repression causing excessive experience-dependent, long-term changes in synaptic function. While this has been hypothesized on the basis of exaggerated mGluR-LTD, it has not been generalized to enhanced plasticity (Bear et al., 2004; Zoghbi and Bear, 2012). The present demonstration, one of the first demonstrating that synaptic transmission and potentiating synaptic plasticity are abnormally enhanced in the absence of FMRP, highlights the importance and value of incorporating behavioral assessment into studies of brain slices to assess cellular and network parameters to understand mechanisms of behavior and cognition.

This study is also one of the first to extend the investigation of the mechanisms of behavior and cognition in FXS to a freely behaving mouse model of the disorder. We find that in freely behaving *Fmr1*-null mice, the basic single-cell electrophysiological properties of dorsal CA1 neurons are normal. Although we classified more single units as putative interneurons in *Fmr1*-null mice and a lower proportion of the putative principal cells as place cells, these differences could easily be due to sampling biases. Importantly, the place cell discharge properties were nonetheless normal, suggesting that complex information processing is also intact (Figure 2). Indeed, the spatial firing properties of *Fmr1*-null and WT place cells were indistinguishable, even across changed environments (Figure S4), and if anything, place fields were better preserved during the challenge of arena rotation (Figure S6) that dissociates space into two distinct spatial

(C) A two-way ANOVA was conducted on the influence of genotype and annular region of the environment on the time spent in each of the eight equal-area annuli. While there was an effect of annulus ($F_{7,56} = 330.49$, $p = 10^{-43}$, $\eta_p^2 = 0.98$), there were no effects of genotype ($F_{1,56} = 1.48$, $p = 0.2$, $\eta_p^2 = 0.025$) or the genotype × annulus interaction ($F_{7,56} = 0.83$, $p = 0.6$, $\eta_p^2 = 0.094$). These lack of differences indicate that WT and *Fmr1*-null mice were not distinct in the ways in which they sampled and moved through the environment in either the presence or the absence of shock.

(D–F) Both WT and *Fmr1*-null mice learned equally well to avoid the shock zone. The genotype × session repeated-measures ANOVA showed no effects of genotype on number of entries (D; $F_{1,28} = 0.045$, $p = 0.8$, $\eta_p^2 = 0.0016$), time-to-first entry (E; $F_{1,28} = 0.10$, $p = 0.8$, $\eta_p^2 = 0.0036$), or shocks/entry (F; $F_{1,28} = 1.19$, $p = 0.28$, $\eta_p^2 = 0.041$), indicating that WT and *Fmr1* null did not differ in ability to learn the location of the shock zone, retain location information across trials, or differ in motivation to escape the shock zone. There was an effect of session on the number of entries ($F_{3,28} = 134.03$, $p = 10^{-18}$, p-$\eta^2 = 0.93$), the time-to-first entry ($F_{3,28} = 12.44$, $p = 10^{-5}$, $\eta_p^2 = 0.57$), and shocks/entry ($F_{3,28} = 147.91$, $p = 10^{-17}$, $\eta_p^2 = 0.94$), but no interaction ($F_{3,28} = 1.14$, $p = 0.4$, $\eta_p^2 = 0.11$; $F_{3,28} = 0.1$, $p = 0.9$, $\eta_p^2 = 0.014$; $F_{3,28} = 0.43$, $p = 0.7$, $\eta_p^2 = 0.044$) on these measures, respectively. These analyses indicate that the groups could not be distinguished in learning to avoid the shock zone.

(G) The two-way ANOVA was conducted on the influence of genotype and 10 min time block on the number of errors (entrances into the former shock zone) for each of the two extinction sessions. During the first extinction session, the effect of block ($F_{2,21} = 4.24$, $p = 0.03$, $\eta_p^2 = 0.29$) was significant, but not the effects of genotype ($F_{1,21} = 1.33$, $p = 0.3$, $\eta_p^2 = 0.06$) or the interaction ($F_{2,21} = 1.39$, $p = 0.3$, $\eta_p^2 = 0.12$), suggesting equivalent extinction learning in WT and *Fmr1*-null mice.

(H) During the second extinction session, there were significant effects of genotype ($F_{1,18} = 7.00$, $p = 0.02$, $\eta_p^2 = 0.28$) and of block ($F_{2,18} = 3.98$, $p = 0.04$, $\eta_p^2 = 0.31$) and no interaction ($F_{2,18} = 0.40$, $p = 0.7$, $\eta_p^2 = 0.043$), indicating that although both genotypes learned throughout the second extinction session, the *Fmr1* null entered the original shock zone less frequently during each time block. This pattern of initially similar WT and *Fmr1* null avoidance, but greater avoidance in the *Fmr1* null during a second extinction session, has been reported (Radwan et al., 2016).

Error bars represent SEM.

frames. Rotation disturbs rat place cells if there has been no spatial training (Zinyuk et al., 2000). While disruption was not observed in non-spatially trained mice (Figure 5; Figure S6), the similarly intact place cell responses of *Fmr1* null and WT mice parallel the intact memory and navigation that *Fmr1*-null mice display (Figure S1) during place avoidance tasks on the rotating arena (Radwan et al., 2016). Indeed, like others (Bakker et al., 1994; Bhattacharya et al., 2012; Brennan et al., 2006; D'Hooge et al., 1997; Zhao et al., 2005), the most reliable cognitive deficit that we have previously detected in *Fmr1*-null mice is cognitive inflexibility. Their ability to update learned avoidance of a shock zone was impaired when the location of shock changed (Radwan et al., 2016; see also Figure 6). If one interprets the hippocampus place code as a dedicated code (see Fenton, 2015a), then these findings directly contradict predictions from disruption hypotheses: place cell cognitive information processing appears normal despite abnormal experience-dependent synaptic function. Importantly, we have argued that the hippocampus place code is not a dedicated code and instead should be interpreted as an ensemble code comprised of neurons with mixed selectivity responses (Fenton et al., 2008; Park et al., 2011; Xie et al., 2016). This interpretation emphasizes the temporal interactions in the discharge between cells, called neural coordination, and deemphasizes single-cell discharge properties, like firing rates and place fields, in light of multimodal response tuning (Buzsáki, 2010; Fenton, 2015a, 2015b; Fusi et al., 2007; Harris et al., 2003; Phillips and Singer, 1997). Indeed, our correlation analyses find that estimates of cognitive performance in the place avoidance task are predicted by estimates of correlated place cell network discharge on the timescales of gamma and theta; no such relationship was identified between cognitive variables and single-cell measures of place field quality (e.g., map coherence: $r = -0.32$, $p = 0.2$, $r^2 = 0.11$, information content: $r = 0.27$, $p = 0.24$, $r^2 = 0.07$). Together, these findings point to the importance of neural coordination as a potential neural measure of cognition and that these can be accomplished by pairwise estimates of the characteristics of higher-order hippocampus network dynamics (Meshulam et al., 2017; Schneidman et al., 2006).

Neural Discoordination in the Hippocampus Network of *Fmr1*-Null Mice

Consistent with alternative hyperstable/discoordination hypotheses that interpret the hippocampus place code as an ensemble code, hippocampal discharge is by no means normal in *Fmr1*-null mice. The substantial abnormalities argue for a different conceptualization of the pathophysiology that can explain cognitive dysfunction in FXS and autism and perhaps other conditions that are characterized by cognitive information-processing deficits (Phillips and Silverstein, 2003; Uhlhaas and Singer, 2007). The coordinated activity between groups of hippocampal principal cells is abnormal in *Fmr1*-null mice, indicating a dissociation between intact single-cell properties and the temporal coordination of their interactions at the level of the hippocampus information-processing network, as predicted by discoordination hypotheses for cognitive dysfunction both generally (Fenton, 2015b; Lee et al., 2014) and in the case of FXS in particular (Radwan et al., 2016). Accordingly, inferences from single-cell properties can be misleading, and instead, it may be the temporally organized interactions among cells that provide informative indicators of cognitive function (Buzsáki, 2010; Fenton, 2015a, 2015b; Johnson et al., 2009; Okun et al., 2015; Suh et al., 2013).

Relationships between the discharge of single CA1 cells and oscillations in the LFP generated by synaptic interactions among large numbers of cells reveal abnormally weak coupling between individual cells and the population in *Fmr1*-null mice (Figure 3B). Furthermore, the set of these weak relationships is abnormally stereotyped. Within this abnormal weakly correlated network state, we also observed a substantially reduced variety of spike-phase relationships between non-spatially tuned cells and theta oscillations in the *Fmr1*-null LFP (Figure 3C). Thus, activity within the *Fmr1*-null hippocampus network of principal cells forms an abnormally invariant and weak spatial firing network infrastructure within which the intact single-cell location-specific activity of place cells is embedded. Because principal cells in hippocampus drive inhibition that organizes network dynamics crucial for information processing (reviewed in Buzsáki, 2010), it is possibly pathological that in *Fmr1*-null mice, there is an increased prevalence of non-spatial pyramidal cells, with spiking that is poorly organized by the ongoing LFP (Figure 3B), forming a relatively functionally homogeneous group of neurons (Figure 3C). This may be one of the contributors to both the weak network states (Figure 4) and the paradoxically rigid single place cell properties of *Fmr1*-null mice during arena rotation (Figure 5).

System-Level Origins of Intellectual Disability in FXS

The interactions between the spike trains of multiple cells provide crucial additional evidence that despite their intact place tuning properties, individual *Fmr1*-null place cells form abnormally weakly coordinated networks at the timescale of inhibition-associated gamma and theta oscillations, as well as an abnormally weakly coordinated network of cells at multiple longer timescales up to a few seconds (Figure 5). Together, these findings provide a novel conceptual picture of intellectual disability in FXS and the associated autistic features; *Fmr1*-null neural circuits are comprised of functionally normal individual cells (Figure 2) that express stereotypically weak discharge relationships to the phases of ongoing oscillations in the LFP and form correspondingly weak network states because they inadequately cohere into common-function neural ensembles (Figures 4 and 5D). This viewpoint can account for findings that basic learning and memory are intact whereas cognitive and memory inflexibility characterize FXS-model mice (Radwan et al., 2016). If correct, this should engender optimism because therapeutic approaches may only need to target the mechanisms of coordination rather than the potentially less easy to manipulate mechanisms that establish and tune the response properties of individual cells.

Going forward, in the pursuit of novel therapies, it will be important to identify proximal mechanisms of the discoordination associated with FMRP absence. Initial clues point to inhibition abnormality in the regulation of spike timing (Anastassiou et al., 2010), more so than increased excitability, which may also explain increased seizure likelihood in the absence of FMRP (Dölen et al., 2007; Zhong et al., 2010).

STAR★METHODS

Detailed methods are provided in the online version of this paper and include the following:

- KEY RESOURCES TABLE
- CONTACT FOR REAGENT AND RESOURCE SHARING
- EXPERIMENTAL MODEL AND SUBJECT DETAILS
- METHOD DETAILS
  - *Ex Vivo* Slice Electrophysiology
  - *In Vivo* Electrophysiology
  - Histology
  - Behavioral Procedures
  - Data Analysis
- QUANTIFICATION AND STATISTICAL ANALYSIS
- DATA AND SOFTWARE AVAILABILITY

SUPPLEMENTAL INFORMATION

Supplemental Information includes six figures and two tables and can be found with this article online at https://doi.org/10.1016/j.neuron.2017.12.043.

ACKNOWLEDGMENTS

The authors are supported by Simons Foundation grant SFARI 294388, NIH grants R01MH099128 to A.A.F. and R21NS091830 to J.M.A., NIMH studentship MH96331-5 to Z.N.T., and a Canadian Institutes of Health Research (CIHR) fellowship 201411MFE-339265-171319 to F.T.S.

AUTHOR CONTRIBUTIONS

F.T.S. and Z.N.T. collected and analyzed place cell data; Z.N.T., D.D., and A.A.F. analyzed spike train data; J.M.A., B.M.C., and A.A.F. collected and analyzed *ex vivo* data; A.A.F. supervised research and wrote the manuscript with contributions from all authors.

DECLARATION OF INTERESTS

The authors declare no competing interests.

Received: May 8, 2017
Revised: October 6, 2017
Accepted: December 27, 2017
Published: January 18, 2018

REFERENCES

Anastassiou, C.A., Montgomery, S.M., Barahona, M., Buzsáki, G., and Koch, C. (2010). The effect of spatially inhomogeneous extracellular electric fields on neurons. J. Neurosci. *30*, 1925–1936.

Bakker, C.E., Verheij, C., Willemsen, R., Vanderhelm, R., Oerlemans, F., Vermey, M., Bygrave, A., Hoogeveen, A.T., Oostra, B.A., Reyniers, E., et al.; The Dutch-Belgian Fragile X Consortium (1994). *Fmr1* knockout mice: a model to study fragile X mental retardation. Cell *78*, 23–33.

Bassell, G.J., and Warren, S.T. (2008). Fragile X syndrome: loss of local mRNA regulation alters synaptic development and function. Neuron *60*, 201–214.

Bear, M.F., Huber, K.M., and Warren, S.T. (2004). The mGluR theory of fragile X mental retardation. Trends Neurosci. *27*, 370–377.

Bhakar, A.L., Dölen, G., and Bear, M.F. (2012). The pathophysiology of fragile X (and what it teaches us about synapses). Annu. Rev. Neurosci. *35*, 417–443.

Bhattacharya, A., Kaphzan, H., Alvarez-Dieppa, A.C., Murphy, J.P., Pierre, P., and Klann, E. (2012). Genetic removal of p70 S6 kinase 1 corrects molecular, synaptic, and behavioral phenotypes in fragile X syndrome mice. Neuron *76*, 325–337.

Braun, K., and Segal, M. (2000). FMRP involvement in formation of synapses among cultured hippocampal neurons. Cereb. Cortex *10*, 1045–1052.

Brennan, F.X., Albeck, D.S., and Paylor, R. (2006). *Fmr1* knockout mice are impaired in a leverpress escape/avoidance task. Genes Brain Behav. *5*, 467–471.

Brown, V., Jin, P., Ceman, S., Darnell, J.C., O'Donnell, W.T., Tenenbaum, S.A., Jin, X., Feng, Y., Wilkinson, K.D., Keene, J.D., et al. (2001). Microarray identification of FMRP-associated brain mRNAs and altered mRNA translational profiles in fragile X syndrome. Cell *107*, 477–487.

Buzsáki, G. (2010). Neural syntax: cell assemblies, synapsembles, and readers. Neuron *68*, 362–385.

Chen, Z., Resnik, E., McFarland, J.M., Sakmann, B., and Mehta, M.R. (2011). Speed controls the amplitude and timing of the hippocampal gamma rhythm. PLoS ONE *6*, e21408.

Chen, T., Lu, J.S., Song, Q., Liu, M.G., Koga, K., Descalzi, G., Li, Y.Q., and Zhuo, M. (2014). Pharmacological rescue of cortical synaptic and network potentiation in a mouse model for fragile X syndrome. Neuropsychopharmacology *39*, 1955–1967.

Cho, Y.H., Giese, K.P., Tanila, H., Silva, A.J., and Eichenbaum, H. (1998). Abnormal hippocampal spatial representations in alphaCaMKIIT286A and CREBalphaDelta- mice. Science *279*, 867–869.

Cimadevilla, J.M., Wesierska, M., Fenton, A.A., and Bures, J. (2001). Inactivating one hippocampus impairs avoidance of a stable room-defined place during dissociation of arena cues from room cues by rotation of the arena. Proc. Natl. Acad. Sci. USA *98*, 3531–3536.

Colak, D., Zaninovic, N., Cohen, M.S., Rosenwaks, Z., Yang, W.-Y., Gerhardt, J., Disney, M.D., and Jaffrey, S.R. (2014). Promoter-bound trinucleotide repeat mRNA drives epigenetic silencing in fragile X syndrome. Science *343*, 1002–1005.

Comery, T.A., Harris, J.B., Willems, P.J., Oostra, B.A., Irwin, S.A., Weiler, I.J., and Greenough, W.T. (1997). Abnormal dendritic spines in fragile X knockout mice: maturation and pruning deficits. Proc. Natl. Acad. Sci. USA *94*, 5401–5404.

D'Hooge, R., Nagels, G., Franck, F., Bakker, C.E., Reyniers, E., Storm, K., Kooy, R.F., Oostra, B.A., Willems, P.J., and De Deyn, P.P. (1997). Mildly impaired water maze performance in male *Fmr1* knockout mice. Neuroscience *76*, 367–376.

Darnell, J.C., Van Driesche, S.J., Zhang, C., Hung, K.Y., Mele, A., Fraser, C.E., Stone, E.F., Chen, C., Fak, J.J., Chi, S.W., et al. (2011). FMRP stalls ribosomal translocation on mRNAs linked to synaptic function and autism. Cell *146*, 247–261.

Deng, P.Y., Sojka, D., and Klyachko, V.A. (2011). Abnormal presynaptic short-term plasticity and information processing in a mouse model of fragile X syndrome. J. Neurosci. *31*, 10971–10982.

Dölen, G., Osterweil, E., Rao, B.S., Smith, G.B., Auerbach, B.D., Chattarji, S., and Bear, M.F. (2007). Correction of fragile X syndrome in mice. Neuron *56*, 955–962.

Dölen, G., Carpenter, R.L., Ocain, T.D., and Bear, M.F. (2010). Mechanism-based approaches to treating fragile X. Pharmacol. Ther. *127*, 78–93.

Dragoi, G., and Tonegawa, S. (2013). Development of schemas revealed by prior experience and NMDA receptor knock-out. eLife *2*, e01326.

Fenton, A.A. (2015a). Coordinating with the "inner GPS". Hippocampus *25*, 763–769.

Fenton, A.A. (2015b). Excitation-inhibition discoordination in rodent models of mental disorders. Biol. Psychiatry *77*, 1079–1088.

Fenton, A.A., and Muller, R.U. (1998). Place cell discharge is extremely variable during individual passes of the rat through the firing field. Proc. Natl. Acad. Sci. USA *95*, 3182–3187.

Fenton, A.A., Kao, H.-Y., Neymotin, S.A., Olypher, A., Vayntrub, Y., Lytton, W.W., and Ludvig, N. (2008). Unmasking the CA1 ensemble place code by exposures to small and large environments: more place cells and multiple, irregularly arranged, and expanded place fields in the larger space. J. Neurosci. *28*, 11250–11262.

Fenton, A.A., Lytton, W.W., Barry, J.M., Lenck-Santini, P.P., Zinyuk, L.E., Kubík, S., Bures, J., Poucet, B., Muller, R.U., and Olypher, A.V. (2010). Attention-like modulation of hippocampus place cell discharge. J. Neurosci. *30*, 4613–4625.

Fox, S.E., and Ranck, J.B., Jr. (1975). Localization and anatomical identification of theta and complex spike cells in dorsal hippocampal formation of rats. Exp. Neurol. *49*, 299–313.

Fox, S.E., and Ranck, J.B., Jr. (1981). Electrophysiological characteristics of hippocampal complex-spike cells and theta cells. Exp. Brain Res. *41*, 399–410.

Franklin, A.V., Rusche, J.R., and McMahon, L.L. (2014). Increased long-term potentiation at medial-perforant path-dentate granule cell synapses induced by selective inhibition of histone deacetylase 3 requires fragile X mental retardation protein. Neurobiol. Learn. Mem. *114*, 193–197.

Fusi, S., Asaad, W.F., Miller, E.K., and Wang, X.J. (2007). A neural circuit model of flexible sensorimotor mapping: learning and forgetting on multiple timescales. Neuron *54*, 319–333.

Gibson, J.R., Bartley, A.F., Hays, S.A., and Huber, K.M. (2008). Imbalance of neocortical excitation and inhibition and altered UP states reflect network hyperexcitability in the mouse model of fragile X syndrome. J. Neurophysiol. *100*, 2615–2626.

Godfraind, J.M., Reyniers, E., De Boulle, K., D'Hooge, R., De Deyn, P.P., Bakker, C.E., Oostra, B.A., Kooy, R.F., and Willems, P.J. (1996). Long-term potentiation in the hippocampus of fragile X knockout mice. Am. J. Med. Genet. *64*, 246–251.

Gross, C., Yao, X., Pong, D.L., Jeromin, A., and Bassell, G.J. (2011). Fragile X mental retardation protein regulates protein expression and mRNA translation of the potassium channel Kv4.2. J. Neurosci. *31*, 5693–5698.

Harris, K.D., Csicsvari, J., Hirase, H., Dragoi, G., and Buzsáki, G. (2003). Organization of cell assemblies in the hippocampus. Nature *424*, 552–556.

Henze, D.A., Borhegyi, Z., Csicsvari, J., Mamiya, A., Harris, K.D., and Buzsáki, G. (2000). Intracellular features predicted by extracellular recordings in the hippocampus in vivo. J. Neurophysiol. *84*, 390–400.

Hok, V., Chah, E., Reilly, R.B., and O'Mara, S.M. (2012). Hippocampal dynamics predict interindividual cognitive differences in rats. J. Neurosci. *32*, 3540–3551.

Hooper, S.R., Hatton, D., Sideris, J., Sullivan, K., Hammer, J., Schaaf, J., Mirrett, P., Ornstein, P.A., and Bailey, D.P., Jr. (2008). Executive functions in young males with fragile X syndrome in comparison to mental age-matched controls: baseline findings from a longitudinal study. Neuropsychology *22*, 36–47.

Hsieh, C., Tsokas, P., Serrano, P., Hernández, A.I., Tian, D., Cottrell, J.E., Shouval, H.Z., Fenton, A.A., and Sacktor, T.C. (2017). Persistent increased PKMζ in long-term and remote spatial memory. Neurobiol. Learn. Mem. *138*, 135–144.

Hu, H., Qin, Y., Bochorishvili, G., Zhu, Y., van Aelst, L., and Zhu, J.J. (2008). Ras signaling mechanisms underlying impaired GluR1-dependent plasticity associated with fragile X syndrome. J. Neurosci. *28*, 7847–7862.

Huber, K.M., Gallagher, S.M., Warren, S.T., and Bear, M.F. (2002). Altered synaptic plasticity in a mouse model of fragile X mental retardation. Proc. Natl. Acad. Sci. USA *99*, 7746–7750.

Hunsaker, M.R., Kim, K., Willemsen, R., and Berman, R.F. (2012). CGG trinucleotide repeat length modulates neural plasticity and spatiotemporal processing in a mouse model of the fragile X premutation. Hippocampus *22*, 2260–2275.

Jackson, J., and Redish, A.D. (2007). Network dynamics of hippocampal cell-assemblies resemble multiple spatial maps within single tasks. Hippocampus *17*, 1209–1229.

Johnson, A., Fenton, A.A., Kentros, C., and Redish, A.D. (2009). Looking for cognition in the structure within the noise. Trends Cogn. Sci. *13*, 55–64.

Kelemen, E., and Fenton, A.A. (2010). Dynamic grouping of hippocampal neural activity during cognitive control of two spatial frames. PLoS Biol. *8*, e1000403.

Kelemen, E., and Fenton, A.A. (2016). Coordinating different representations in the hippocampus. Neurobiol. Learn. Mem. *129*, 50–59.

Kooy, R.F., D'Hooge, R., Reyniers, E., Bakker, C.E., Nagels, G., De Boulle, K., Storm, K., Clincke, G., De Deyn, P.P., Oostra, B.A., and Willems, P.J. (1996). Transgenic mouse model for the fragile X syndrome. Am. J. Med. Genet. *64*, 241–245.

Krueger, D.D., Osterweil, E.K., Chen, S.P., Tye, L.D., and Bear, M.F. (2011). Cognitive dysfunction and prefrontal synaptic abnormalities in a mouse model of fragile X syndrome. Proc. Natl. Acad. Sci. USA *108*, 2587–2592.

Kubík, S., and Fenton, A.A. (2005). Behavioral evidence that segregation and representation are dissociable hippocampal functions. J. Neurosci. *25*, 9205–9212.

Larson, J., Jessen, R.E., Kim, D., Fine, A.K., and du Hoffmann, J. (2005). Age-dependent and selective impairment of long-term potentiation in the anterior piriform cortex of mice lacking the fragile X mental retardation protein. J. Neurosci. *25*, 9460–9469.

Laughlin, R.B., Pines, D., Schmalian, J., Stojkovic, B.P., and Wolynes, P. (2000). The middle way. Proc. Natl. Acad. Sci. USA *97*, 32–37.

Lauterborn, J.C., Rex, C.S., Kramár, E., Chen, L.Y., Pandyarajan, V., Lynch, G., and Gall, C.M. (2007). Brain-derived neurotrophic factor rescues synaptic plasticity in a mouse model of fragile X syndrome. J. Neurosci. *27*, 10685–10694.

Lee, H., Dvorak, D., and Fenton, A.A. (2014). Targeting neural synchrony deficits is sufficient to improve cognition in a schizophrenia-related neurodevelopmental model. Front. Psychiatry *5*, 15.

Lumley, T., Diehr, P., Emerson, S., and Chen, L. (2002). The importance of the normality assumption in large public health data sets. Annu. Rev. Public Health *23*, 151–169.

Maurer, A.P., Cowen, S.L., Burke, S.N., Barnes, C.A., and McNaughton, B.L. (2006). Organization of hippocampal cell assemblies based on theta phase precession. Hippocampus *16*, 785–794.

McFarland, W.L., Teitelbaum, H., and Hedges, E.K. (1975). Relationship between hippocampal theta activity and running speed in the rat. J. Comp. Physiol. Psychol. *88*, 324–328.

McHugh, T.J., Blum, K.I., Tsien, J.Z., Tonegawa, S., and Wilson, M.A. (1996). Impaired hippocampal representation of space in CA1-specific NMDAR1 knockout mice. Cell *87*, 1339–1349.

McHugh, T.J., Jones, M.W., Quinn, J.J., Balthasar, N., Coppari, R., Elmquist, J.K., Lowell, B.B., Fanselow, M.S., Wilson, M.A., and Tonegawa, S. (2007). Dentate gyrus NMDA receptors mediate rapid pattern separation in the hippocampal network. Science *317*, 94–99.

Meshulam, L., Gauthier, J.L., Brody, C.D., Tank, D.W., and Bialek, W. (2017). Collective behavior of place and non-place neurons in the hippocampal network. Neuron *96*, 1178–1191.e4.

Moser, M.B., Rowland, D.C., and Moser, E.I. (2015). Place cells, grid cells, and memory. Cold Spring Harb. Perspect. Biol. *7*, a021808.

Muller, R.U., and Kubie, J.L. (1989). The firing of hippocampal place cells predicts the future position of freely moving rats. J. Neurosci. *9*, 4101–4110.

Nakazawa, K., Quirk, M.C., Chitwood, R.A., Watanabe, M., Yeckel, M.F., Sun, L.D., Kato, A., Carr, C.A., Johnston, D., Wilson, M.A., and Tonegawa, S. (2002). Requirement for hippocampal CA3 NMDA receptors in associative memory recall. Science *297*, 211–218.

Nakazawa, K., Sun, L.D., Quirk, M.C., Rondi-Reig, L., Wilson, M.A., and Tonegawa, S. (2003). Hippocampal CA3 NMDA receptors are crucial for memory acquisition of one-time experience. Neuron *38*, 305–315.

Neymotin, S.A., Lytton, W.W., Olypher, A.V., and Fenton, A.A. (2011). Measuring the quality of neuronal identification in ensemble recordings. J. Neurosci. *31*, 16398–16409.

Neymotin, S.A., Talbot, Z.N., Jung, J.Q., Fenton, A.A., and Lytton, W.W. (2017). Tracking recurrence of correlation structure in neuronal recordings. J. Neurosci. Methods *275*, 1–9.

O'Keefe, J., and Nadel, L. (1978). The Hippocampus as a Cognitive Map (Clarendon Press).

Okun, M., Steinmetz, N., Cossell, L., Iacaruso, M.F., Ko, H., Barthó, P., Moore, T., Hofer, S.B., Mrsic-Flogel, T.D., Carandini, M., and Harris, K.D. (2015). Diverse coupling of neurons to populations in sensory cortex. Nature *521*, 511–515.

Park, E., Dvorak, D., and Fenton, A.A. (2011). Ensemble place codes in hippocampus: CA1, CA3, and dentate gyrus place cells have multiple place fields in large environments. PLoS ONE *6*, e22349.

Park, E.H., Burghardt, N.S., Dvorak, D., Hen, R., and Fenton, A.A. (2015). Experience-dependent regulation of dentate gyrus excitability by adult-born granule cells. J. Neurosci. *35*, 11656–11666.

Pastalkova, E., Serrano, P., Pinkhasova, D., Wallace, E., Fenton, A.A., and Sacktor, T.C. (2006). Storage of spatial information by the maintenance mechanism of LTP. Science *313*, 1141–1144.

Patel, A.B., Hays, S.A., Bureau, I., Huber, K.M., and Gibson, J.R. (2013). A target cell-specific role for presynaptic *Fmr1* in regulating glutamate release onto neocortical fast-spiking inhibitory neurons. J. Neurosci. *33*, 2593–2604.

Pavlowsky, A., Wallace, E., Fenton, A.A., and Alarcon, J.M. (2017). Persistent modifications of hippocampal synaptic function during remote spatial memory. Neurobiol. Learn. Mem. *138*, 182–197.

Phillips, W.A., and Silverstein, S.M. (2003). Convergence of biological and psychological perspectives on cognitive coordination in schizophrenia. Behav. Brain Sci. *26*, 65–82, discussion 82–137.

Phillips, W.A., and Singer, W. (1997). In search of common foundations for cortical computation. Behav. Brain Sci. *20*, 657–683, discussion 683–722.

Pieretti, M., Zhang, F.P., Fu, Y.H., Warren, S.T., Oostra, B.A., Caskey, C.T., and Nelson, D.L. (1991). Absence of expression of the FMR-1 gene in fragile X syndrome. Cell *66*, 817–822.

Radwan, B., Dvorak, D., and Fenton, A.A. (2016). Impaired cognitive discrimination and discoordination of coupled theta-gamma oscillations in *Fmr1* knockout mice. Neurobiol. Dis. *88*, 125–138.

Ranck, J.B., Jr. (1973). Studies on single neurons in dorsal hippocampal formation and septum in unrestrained rats. I. Behavioral correlates and firing repertoires. Exp. Neurol. *41*, 461–531.

Ratcliffe, J.F. (1968). The effect on the t distribution of non-normality in the sampled population. J. R. Stat. Soc. Ser. C Appl. Stat. *17*, 42–48.

Rotenberg, A., Mayford, M., Hawkins, R.D., Kandel, E.R., and Muller, R.U. (1996). Mice expressing activated CaMKII lack low frequency LTP and do not form stable place cells in the CA1 region of the hippocampus. Cell *87*, 1351–1361.

Rotenberg, A., Abel, T., Hawkins, R.D., Kandel, E.R., and Muller, R.U. (2000). Parallel instabilities of long-term potentiation, place cells, and learning caused by decreased protein kinase A activity. J. Neurosci. *20*, 8096–8102.

Schneidman, E., Berry, M.J., 2nd, Segev, R., and Bialek, W. (2006). Weak pairwise correlations imply strongly correlated network states in a neural population. Nature *440*, 1007–1012.

Skaggs, W.E., McNaughton, B.L., Gothard, K.M., and Markus, E.J. (1993). An information theoretic approach to deciphering the hippocampal code. In Advances in Neural Information Processing, S.J. Hanson, J.D. Cowan, and C.L. Giles, eds. (Morgan Kaufmann Publishers), pp. 1030–1037.

Sørensen, E.M., Bertelsen, F., Weikop, P., Skovborg, M.M., Banke, T., Drasbek, K.R., and Scheel-Krüger, J. (2015). Hyperactivity and lack of social discrimination in the adolescent *Fmr1* knockout mouse. Behav. Pharmacol. *26*, 733–740.

Sparks, F.T., Talbot, Z.N., Dvorak, D., and Fenton, A.A. (2018). Extracellular CA1 spike trains recorded from Fmr1-null and wild-type mice during free exploration in a variety of environments that include a small and a large box, a ring, and a circular open field that is either stationary or rotating. CRCNS.org. https://doi.org/10.6080/K01V5C44.

Suh, J., Foster, D.J., Davoudi, H., Wilson, M.A., and Tonegawa, S. (2013). Impaired hippocampal ripple-associated replay in a mouse model of schizophrenia. Neuron *80*, 484–493.

Tsokas, P., Hsieh, C., Yao, Y., Lesburguères, E., Wallace, E.J.C., Tcherepanov, A., Jothianandan, D., Hartley, B.R., Pan, L., Rivard, B., et al. (2016). Compensation for PKMζ in long-term potentiation and spatial long-term memory in mutant mice. eLife *5*, 5.

Uhlhaas, P.J., and Singer, W. (2007). What do disturbances in neural synchrony tell us about autism? Biol. Psychiatry *62*, 190–191.

Voigts, J., Siegle, J.H., Pritchett, D.L., and Moore, C.I. (2013). The flexDrive: an ultra-light implant for optical control and highly parallel chronic recording of neuronal ensembles in freely moving mice. Front. Syst. Neurosci. *7*, 8.

Waung, M.W., and Huber, K.M. (2009). Protein translation in synaptic plasticity: mGluR-LTD, Fragile X. Curr. Opin. Neurobiol. *19*, 319–326.

Xie, K., Fox, G.E., Liu, J., Lyu, C., Lee, J.C., Kuang, H., Jacobs, S., Li, M., Liu, T., Song, S., and Tsien, J.Z. (2016). Brain computation is organized via power-of-two-based permutation logic. Front. Syst. Neurosci. *10*, 95.

Yun, S.H., and Trommer, B.L. (2011). Fragile X mice: reduced long-term potentiation and N-Methyl-D-Aspartate receptor-mediated neurotransmission in dentate gyrus. J. Neurosci. Res. *89*, 176–182.

Zhang, L., and Alger, B.E. (2010). Enhanced endocannabinoid signaling elevates neuronal excitability in fragile X syndrome. J. Neurosci. *30*, 5724–5729.

Zhao, M.G., Toyoda, H., Ko, S.W., Ding, H.K., Wu, L.J., and Zhuo, M. (2005). Deficits in trace fear memory and long-term potentiation in a mouse model for fragile X syndrome. J. Neurosci. *25*, 7385–7392.

Zhong, J., Chuang, S.C., Bianchi, R., Zhao, W., Paul, G., Thakkar, P., Liu, D., Fenton, A.A., Wong, R.K., and Tiedge, H. (2010). Regulatory BC1 RNA and the fragile X mental retardation protein: convergent functionality in brain. PLoS ONE *5*, e15509.

Zinyuk, L., Kubik, S., Kaminsky, Y., Fenton, A.A., and Bures, J. (2000). Understanding hippocampal activity by using purposeful behavior: place navigation induces place cell discharge in both task-relevant and task-irrelevant spatial reference frames. Proc. Natl. Acad. Sci. USA *97*, 3771–3776.

Zoghbi, H.Y., and Bear, M.F. (2012). Synaptic dysfunction in neurodevelopmental disorders associated with autism and intellectual disabilities. Cold Spring Harb. Perspect. Biol. *4*, 4.

STAR★METHODS

KEY RESOURCES TABLE

REAGENT or RESOURCE	SOURCE	IDENTIFIER
Deposited Data		
Raw data	This paper	https://doi.org/10.6080/K01V5C44
Experimental Models: Organisms/Strains		
Mouse: B6.129P2-Fmr1$^{tm1Cgr/J}$	The Jackson Laboratory	JAX: 003025; RRID: IMSR_JAX:003025
Software and Algorithms		
Data acquisition software: DacqUSB	Axona	v.1.2.2
Data acquisition software: Tracker	Bio-Signal Group	v.2.37
Analysis software: TrackAnalysis	Bio-Signal Group	v.2.52
Analysis code: Phase Frequency Spike Probability Plots As in Figures 3 and S5	Fenton Lab	https://github.com/FentonLab/SpikeField
Analysis code: Compute Kendall's tau among pairs of spike trains in a BPF file as in Figure 4	Fenton Lab	https://github.com/FentonLab/CorrelateBPFSpikeTrainEpisodes
Analysis code: Compute the Ipos (momentary positional information) time series for the spike trains in a BPF file as in Figure 5	Fenton Lab	https://github.com/FentonLab/PositionalInfo

CONTACT FOR REAGENT AND RESOURCE SHARING

Further information and requests for resources and reagents should be directed to the Lead Contact André Fenton (afenton@nyu.edu).

EXPERIMENTAL MODEL AND SUBJECT DETAILS

Wild-type mice with a mixed C57BL6/129 background were used as well as *Fmr1* null mice carrying the *Fmr1*^{tm1Cgr} allele on the same mixed C57BL6/129 background (Jackson Lab strain number 003025). The mutant mice were obtained from Jackson Laboratories (Bar Harbor, ME) to establish local colonies, and housed in a room with a 12-hr light/dark cycle (light on at 7 am) with access to food and water *ad libitum*. All experimental procedures were performed as approved by the Institutional Animal Care and Use Committees of NYU and the SUNY, Downstate Medical Center, and according to NIH and institutional guidelines and the Public Health Service Policy on Humane Care and Use of Laboratory Animals.

METHOD DETAILS

Ex Vivo Slice Electrophysiology

Male WT (n = 22) and *Fmr1* null mice (n = 26) aged 3-4 months were anesthetized with isoflurane (5% in 100% O_2 for 3 min) 30 min after behavioral examination. They were rapidly decapitated and the brain removed to obtain transverse hippocampal slices (400 μm) from the right dorsal hippocampus. Slices were incubated for 2 hr in oxygenated aCSF (in mM: 119 NaCl, 4.9 KCl, 1.5 $MgSO_4$, 2.5 $CaCl_2$, 26.2 $NaHCO_3$, 1 NaH_2PO_4 and 11 Glucose saturated with 95% O_2, 5% CO_2), and then were placed in a submerged chamber subfused with aCSF at 35-36°C for recording. A pair of stimulation (bipolar; FHC & Co, ME, USA) and recording electrodes (borosilicate glass pipette filled with aCSF; 5-10 MΩ) was used to evoke and record field excitatory postsynaptic potentials (fEPSP) at the CA1 *stratum radiatum*. Stimulus-response curves were obtained by delivering square pulses (50 μs) at increasing voltages (0-40 V). For synaptic potentiation studies, the test pulse intensity was set at 40% of the maximum fEPSP slope amplitude and sampled once per minute. After a stable baseline response was established, a single 1 s 100-Hz stimulation (high-frequency stimulation, HFS) was delivered to induce long-lasting potentiation. All datasets were normalized to baseline (pre-HFS) values. Slope amplitudes between conditions were compared at three phases of potentiation relative to the baseline: i) post-tetanic potentiation (PTP) measured by averaging during the first 8 min after HFS, early-potentiation measured by averaging during the 10-20 min after HFS, and late-potentiation measured by averaging during 50-60 min after HFS, measured relative to the 10 min baseline before HFS.

In Vivo Electrophysiology

Male WT (n = 12) and *Fmr1* null mice (n = 9) aged 4-6 months were anesthetized by isoflurane inhalation (1.5% with 1 L/min oxygen) and implanted with a microdrive. Either a customized 8-tetrode Open Ephys Flexdrive (http://www.open-ephys.org; Voigts et al., 2013) or a 4-tetrode customized Versadrive (Neuralynx, Bozeman, MT) was used. Tetrodes were aimed at the dorsal hippocampus (−2.0 mm posterior to bregma, ± 1.75 mm lateral from midline). The Flexdrive targeted both hippocampi. The tetrodes were constructed from 18-μm Nichrome or Platinum Iridium wire and the tips were plated with gold or platinum, respectively, to reduce impedances to 200-250 kOhms. The microdrive was secured to the skull using bone screws and dental cement; one screw served as the ground electrode. The mouse recovered for at least a week before electrophysiological procedures began.

Tetrodes were slowly advanced over two weeks until hippocampal single units could be identified. An electrode without single unit activity was selected as a reference. Extracellular action potential signals were amplified 4-12k times and 0.6-6 kHz band-pass filtered. LFP signals from the same electrodes were amplified 1000 times and 0.1-500 Hz band-pass filtered. Electrophysiology data were recorded using a 64-channel Axona recording system (Axona, St. Albans, UK).

Histology

After data collection concluded, the mice were euthanized by pentobarbital overdose. The mice were transcardially perfused with 4% formalin, brains removed, cryoprotected with 30% sucrose, sliced at 30 μm with a cryostat, and mounted on slides. Cresyl violet stain was used to determine the recording site for each tetrode, which had been targeted to the pyramidal cell layer of CA1.

Behavioral Procedures

Constant Conditions Open-Field and Disk Rotation

Four recording environments were used 1) a small box (28.5 w x 28.5 l x 17 h cm), 2) a large box with black walls (50 w x 50 l x 25 h cm), white acrylic floor, and a checkerboard card attached to one wall, 3) a 10-cm wide, ring with 40-cm outer diameter, and 4) a circular disk-shaped arena (40 cm diameter, 30 cm transparent wall) that could rotate at 0.75 rpm.

Electrophysiology recordings were performed while the mouse explored the small or large boxes, the ring or the disk that was positioned in the same location within the center of the room. A black curtain containing visual orienting cues was placed around the apparatus. The animal's position was tracked at 30 frames/s using an overhead camera and software (Tracker, Bio-Signal Group, Acton, MA) to detect a pair of infrared diodes attached to the animal's microdrive. During arena rotation sessions, position was tracked in both the spatial frame of the room and the spatial frame of the arena. Tracking in the arena frame was performed relative to an infrared diode that was attached to the rotating arena but inaccessible to the animals.

Active Place Avoidance

For *ex vivo* physiology (Figure 1; Figure S1), male WT and *Fmr1* null mice aged 3-4 months were trained in a hippocampus-dependent two-frame active place avoidance task, consisting of a 40-cm diameter arena with a parallel rod floor that rotated at 1 rpm. The position of the animal was tracked as described above. Mice in the trained condition learned the "Room+Arena-" task variant, in which avoiding a 60° sector was reinforced by a constant current foot shock (60 Hz, 500 ms, 0.2 mA) that was scrambled (5-poles) across pairs of the floor rods, triggered by entering the shock zone for more than 500 ms. Additional shocks occurred every 1.5 s until escape. Measures of place avoidance were computed by software (TrackAnalysis, Bio-Signal Group, Acton, MA). Although TrackAnalysis returns a large number of performance measures, to assess place avoidance and to relate it to estimates of hippocampal function, we used the most commonly used and straightforward estimate of place avoidance, the number of errors (entrances to the shock zone) that were observed during a session. The behavioral protocol began with a 10-min session with shock off to habituate the mice to the rotating arena (pretrain). 1 hr later, three 10-min training sessions (60-min inter-trial interval) followed with the shock turned on. An additional conditioning session "24-hr Retest" was performed the following day. Conditions were identical across all sessions except shock was off during pretraining.

For mice used for *in vivo* single unit and LFP recording, male WT and *Fmr1* null mice aged 4-6 months were trained following similar procedures detailed above with the following differences. Mice received foot shock through a copper mesh arena floor, the sessions were 30-min, and inter-session intervals 1.5-hr (Figure 6), and shock was off during extinction.

Data Analysis

Classification of Cell Types

Manual single unit isolation was performed using Wclust software (A.A. Fenton) to define clusters of action potential waveshape parameters in the high-dimensional waveshape parameter space (Figure S2). The quality of this isolation was quantified using $Isol_{BG}$ and $Isol_{NN}$ (Neymotin et al., 2011). These information theoretic measures are computed as the amount that a cluster's identity reduces uncertainty of the 8 most effectively discriminating waveform parameter values. To compute $Isol_{BG}$ the cluster is compared to all other action potentials, and in the case of $Isol_{NN}$, the cluster is compared to the action potentials of the most similar (i.e., the nearest neighbor) cluster in the parameter space. Single units were considered sufficiently well isolated for study only if $Isol_{BG} \geq 4$ bits and $Isol_{NN} \geq 4$ bits, which are criteria that were validated against the ground truth of simultaneous intra- and extracellular action potential recordings (Henze et al., 2000; Neymotin et al., 2011). Single units were classified as complex-spike or theta cells according to published criteria (Fenton et al., 2008; Ranck, 1973) (Figure S3). Complex-spike cells appear to be pyramidal cells, whereas theta cells are likely local interneurons (Fox and Ranck, 1975). Pyramidal cells were judged to have long-duration

waveforms (>250 μs), low discharge rate (<2 AP/s) and a tendency to fire in bursts (peak inter-spike interval < 10 ms). Interneurons had short-duration waveforms (<250 μs), high discharge rate (>2 AP/s), and were less likely to fire in bursts.

Characterization of Place Cells

Cell-specific spatial firing rate maps were created by calculating the total number of spikes observed in each 1.25 × 1.25 cm location, divided by the total time the mouse was in the location. Three qualities of spatial firing were computed from the firing rate map: the overall firing rate is the total spikes a cell discharged divided by the total recording time; spatial coherence describes the local smoothness of the firing rate distribution (Muller and Kubie, 1989); and spatial information content describes the reduction in uncertainty of the mouse's position in the firing rate map given a particular firing rate (Skaggs et al., 1993). Single units were classified as place cells if the overall discharge rate was (0.1-2 AP/s), the spatial coherence (z score) was >0.4, and the information content was >0.4 bits/spike. The spatial similarity of two firing rate maps was computed as Fischer's z-transformation of Pearson's correlation for the firing rates in corresponding pixels of the two maps. The proportion of pixels in which the cell discharged was also computed. Note that while this measure is related to the size of a firing field, it does not directly measure firing fields and thus makes none of the arbitrary assumptions that are required to define a firing field, such as the firing rate threshold that distinguishes between in-field and out-of-field firing, nor does the measure rely on spatial smoothing or other such manipulations that make quantitative firing field definitions subjective, as discussed in Maurer et al. (2006), and perhaps even inappropriate for understanding place coding (Meshulam et al., 2017).

Overdispersion

Overdispersion is the variance of a cell's standardized firing rates for passes through the firing field (Fenton et al., 2010). The standardized firing rate (z) was computed for each 5 s interval as:

$$z = \frac{obs - \exp}{\sqrt{\exp}}$$

where *obs* is the number of observed action potentials and *exp* is the expected number on the assumption of Poisson firing. The expectation is the sum of the product of the time spent (t_i) in a location during time interval i and the time-averaged rate at that location (r_i) computed for all locations that were visited during the 5 s. Note that $exp = 0$ and z is undefined if the mouse does not visit the firing field during a 5 s interval. Only 5 s intervals when the mouse sampled a cell's firing field well were studied. These were identified by $exp \geq$ average rate for the cell (Fenton et al., 2010). To study discharge covariations between pairs of cells, we selected 5 s epochs when the mouse crossed the firing fields of both cells as epochs when expected spatial firing (*exp*) of each cell was above the individual cell's average rate.

Functional Coupling of Cell Pairs

The functional coupling of spike trains from pairs of cells was estimated using Kendall's correlation (Neymotin et al., 2017). The time series was generated by counting the number of spikes the cell fired during each time interval. We examined gamma (25 and 40 ms), theta (125 and 250 ms), as well as 1 s and 5 s (time to cross place field) intervals. Distributions of the population of pairwise correlations within an ensemble of cells are called PCorr, which is the vector of pairwise correlations. PCorr captures higher-order network correlations, as weak pairwise correlations imply strong network states (Schneidman et al., 2006). We used PCo, the Pearson correlation of a pair of PCorr vectors to describe the recurrence of these network states (Neymotin et al., 2017).

Frame-Specific Spatial Firing Analysis

During arena rotation, spatial discharge of a neuron can be represented in either the stationary spatial frame of the room or the rotating spatial frame of the arena. At each moment, discharge can signal location in one frame or the other. To decode which spatial frame is being represented by location-specific CA1 discharge, we computed the momentary positional information I_{pos} as described previously (Kelemen and Fenton, 2010). $I_{pos}(t)$ estimates the location-specific firing of a cell during a brief time interval ($\Delta t = 133$ ms). It is defined as:

$$I_{pos}(t) = p_{i|x} \log_2 \left(\frac{p_{i|x}}{p_i} \right) \quad (1)$$

p_i is the probability of the cell firing i spikes during the interval; $p_{i|x}$ is the probability of firing i spikes if the mouse is in location x. Although $I_{pos}(t)$ can be positive or negative, the absolute value is large whenever the number of spikes observed at the location is distinct or "surprising" compared to the location-independent probability of observing the same number of spikes. The value $\left| I_{pos}(t) \right|$ is given the shorthand, I_{pos}.

A cell's spatial frame preference was estimated by first calculating I_{pos} separately for each spatial frame, then by computing the difference $\Delta I_{pos} = I_{pos(room)} - I_{pos(arena)}$.

To estimate ensemble $I_{pos}(t)$, we first computed the frame-specific sum of the $I_{pos}(t)$ values at each moment. The ensemble difference ΔI_{pos} between the room and arena frame was computed at each time interval to estimate the momentary frame preference in the ensemble discharge. The Pearson correlation between the time series of ensemble ΔI_{pos} values and the time series of an individual cell's ΔI_{pos} values was used to estimate the coordination between an ensemble and a single cell's frame-specific fluctuations in positional information. This coordination was estimated for each cell in the ensemble by computing the ensemble ΔI_{pos} time series after leaving the cell out of the ensemble.

Spike-Field Coordination

Phase-frequency discharge probability plots were computed to characterize the likelihood that a cell's discharge is phase-organized by frequency-specific oscillations in the LFP. For each analysis, the LFP and spike were recorded from the same tetrode, the tetrode wire with the fewest artifacts was selected for the LFP analysis. The LFP signal was convolved with a group of complex Morlet wavelets in the logarithmic range between 2 and 100 Hz. The instantaneous phase of the frequency band-specific LFP signals was obtained from the complex time series. The oscillation phase discharge probability was computed independently for each frequency band. The frequency-specific phase distribution of spiking was normalized by dividing the discharge distribution by the total number of action potentials in a given recording.

QUANTIFICATION AND STATISTICAL ANALYSIS

Average ± SEM values are reported throughout the manuscript. Statistical evaluation of data in figures is presented in the legend. Parametric comparisons of the two genotypes were performed by t test, which because of the Central Limit Theorem is valid and robust even when the normality assumption is violated so long as the sample sizes are large enough (Lumley et al., 2002). Sample sizes greater than 30 tend to be large enough and sizes of 50 are sufficient for skewed distributions (Ratcliffe, 1968). Statistical comparisons in the present work were based on sample distributions with $n > 50$, making them sufficiently large for the validity of the parametric t test (and ANOVA). Nonetheless, because non-parametric tests of inference are commonly used when sample normality is violated, we also report the Mann-Whitney-Wilcoxon test statistic U when both samples are not normally distributed according to the Shapiro-Wilk test. Comparisons of binomial proportions used the proportions z test. Multiple factor comparisons were performed by ANOVA, with repeated-measures, followed by Tukey post hoc tests as appropriate. Statistical comparisons between distributions of correlations (r) were performed on Fisher z-transformed correlation values $z = (1/2)ln(((1+r))/(1+r))$. Significance was set at $p < 0.05$.

DATA AND SOFTWARE AVAILABILITY

Spike train data are available from CRCNS.org (Sparks et al., 2018). Custom code for spike train analyses found in Figures 3, 4, 5 and S5 can be found on GitHub (see Key Resources Table). Further information and requests for data and code used for spike analyses should be directed to the Lead Contact André Fenton (afenton@nyu.edu).